Functionally-Coupled Ion Channels Begin Co-assembling at the Start of Their Synthesis

Authors:

Roya Pournejati[1,2], Jessica M. Huang[1,2], Michael Ma[1,2], Claudia M. Moreno[2,3], Oscar Vivas[1,2]*

Affiliations:

[1] Department of Pharmacology, University of Washington

[2] Department of Neurobiology and Biophysics, University of Washington

[3] Howard Hughes Medical Institute

***Corresponding author:**

Oscar Vivas

Department of Pharmacology

Department of Neurobiology and Biophysics

University of Washington, School of Medicine

Box 357290

Seattle, WA 98195-7290

Email: vivas@uw.edu

Phone: (206) 543-0958

Summary

Calcium binding to BK channels lowers BK activation threshold, substantiating functional coupling with calcium-permeable channels. This coupling requires close proximity between different channel types, and the formation of BK–$Ca_V1.3$ hetero-clusters at nanometer distances exemplifies this unique organization. To investigate the structural basis of this interaction, we tested the hypothesis that BK and $Ca_V1.3$ channels assemble before their insertion into the plasma membrane. Our approach incorporated four strategies: (1) detecting interactions between BK and $Ca_V1.3$ proteins inside the cell, (2) identifying membrane compartments where intracellular hetero-clusters reside, (3) measuring the proximity of their mRNAs, and (4) assessing protein interactions at the plasma membrane during early translation. These analyses revealed that a subset of BK and $Ca_V1.3$ transcripts are spatially close in micro-translational complexes, and their newly synthesized proteins associate within the endoplasmic reticulum (ER) and Golgi. Comparisons with other proteins, transcripts, and randomized localization models support the conclusion that BK and $Ca_V1.3$ hetero-clusters form before their insertion at the plasma membrane.

Significance statement

This work examines the proximity between BK and $Ca_V1.3$ molecules at the level of their mRNAs and newly synthesized proteins to reveal that these channels interact early in their biogenesis. Two cell models were used: a heterologous expression system to investigate the steps of protein trafficking and a pancreatic beta cell line to study the localization of endogenous channel mRNAs. Our findings show that BK and $Ca_V1.3$ channels begin assembling intracellularly before reaching the plasma membrane, revealing new aspects of their spatial organization. This intracellular assembly suggests a coordinated process that contributes to functional coupling.

53 **Introduction**

54 This work concerns the organization of functionally coupled voltage- and calcium-
55 dependent potassium (BK) channels and voltage-gated calcium (Ca_V) channels.

56 BK channels (a.k.a. $K_{Ca}1.1$, Maxi-K, Slo1, KCNMA1) are named for their "big potassium
57 (K^+)" conductance, since channel opening leads to unusually large, outward potassium currents
58 and membrane repolarization. Its amino acid sequence is conserved throughout the animal
59 kingdom from worms to mammals. BK channels are expressed in a wide variety of cell types,
60 predominantly excitable cells but also non-excitable salivary, bone and kidney cells, making this
61 channel responsible for a large range of physiological processes [1-9]. Phenotypes of pathological
62 BK mutations in human patients are most prominent in the brain and muscle and often manifest
63 as seizures, movement disorders, developmental delay, and intellectual disability [10, 11]. BK is
64 also implicated in other organ system functions, including but not limited to heart pace making,
65 reproduction, and pancreatic glucose homeostasis [11, 12].

66 Since BK channels affect function in numerous physiological systems, channel opening is
67 meticulously regulated at the cellular level. BK is a voltage-gated channel activated by membrane
68 depolarization. Interestingly, BK has an additional gating mechanism that differentiates it from
69 typical voltage-gated potassium channels; BK opening is gated by both voltage and intracellular
70 calcium binding to a cytosolic regulatory domain. At the cytoplasmic resting free calcium
71 concentration (~0.1 μM), BK channels remain closed [13]. However, the probability of channel
72 opening increases when both the membrane potential depolarizes and when the local free
73 calcium rises. Yet, increases of calcium are tightly limited by endogenous proteins that bind
74 calcium with high affinity as well as by extrusion mechanisms that take calcium inside organelles
75 or outside the cell. Hence, the activation of BK channels relies on strategies to overcome these
76 regulatory barriers. One such strategy is to localize near sources of calcium.

77 In excitable cells, BK forms nanodomains with calcium channels that provide exclusive,
78 localized calcium sources. Several subtypes of calcium channels form functional signaling
79 complexes with BK, shifting BK activation voltages to more negative potentials [14-16]. One of
80 these channels, $Ca_V1.3$ (a.k.a. *CACNA1D*), is unique in its electrophysiological profile as an L-
81 type calcium channel, activating with fast kinetics at voltages as negative as -55 mV [17].
82 Additionally, BK channels are modulated by auxiliary subunits, which fine-tune BK channel gating
83 properties to adapt to different physiological conditions. The β, γ,

84 and LINGO1 subunits each contribute distinct structural and regulatory features: β-
85 subunits modulate Ca^{2+} sensitivity and can induce inactivation; γ-subunits shift voltage-dependent
86 activation to more negative potentials; and LINGO1 reduces surface expression and promotes

87 rapid inactivation. These interactions ensure precise control over channel activity, allowing BK
88 channels to integrate voltage and calcium signals dynamically in various cell types [18-24].
89 Here, we focus on the selective assembly of BK channels with $Ca_V1.3$ and do not evaluate
90 the contributions of auxiliary subunits to BK channel organization. $Ca_V1.3$ is expressed in many
91 of the same cell types as BK and is often functionally coupled with BK channels, enabling BK
92 channels to activate at more negative voltages. Notably, super-resolution microscopy shows that
93 $Ca_V1.3$ organizes spatially into nanodomains with BK in the plasma membrane [15]. However, the
94 mechanisms behind the assembly of BK and $Ca_V1.3$ hetero-clusters are unknown.
95 Several mechanisms for bringing ion channels together have been suggested (Table 1).
96 One proposes that proteins assembly precedes protein insertion into the plasma membrane [25,
97 26, 31]. This mechanism has been observed in studies of hetero-multimers and even channels
98 permeating different ions. The formation of these groups of proteins would start from their
99 synthesis. There is even the possibility of mRNA transcripts colocalizing prior to translation. We
100 explored this mechanism in relation to BK and $Ca_V1.3$ functional coupling. Here, we started by
101 investigating when and where BK and $Ca_V1.3$ channels cluster in the cell. We looked for BK and

Mechanism	Description	Source
Co-translation of heteromeric channel subunits	mRNA transcripts and nascent proteins of hERG heteromeric subunits form molecular complexes during protein translation.	[25]
Co-translation of channels permeating different ions	Potassium channel hERG and sodium channel SCN5A form complexes of mRNA transcripts and nascent proteins during protein translation.	[26]
Membrane curvature sensing	Clusters of Piezo1 channels enriche in membrane invaginations.	[27]
ER membrane protein complex	ER membrane complex acts as a chaperone for heteromeric channel assembly	[28]
Scaffolding proteins	Scaffolding protein AKAP150 is required for abnormal gating of $Ca_V1.2$-LQT8 channels.	[29]
Random insertion	Clusters of $Ca_V1.2$, $Ca_V1.3$, BK, and TRPV4 are proposed to be randomly formed into the plasma membranes of smooth muscle, cardiac muscle, hippocampal neurons, and tsA-201 cells.	[30]

Table 1. List of mechanisms described for the interaction between channel subunits, channels of the same type (homo-clusters), or hetero-clusters of channel families permeating different ions.

102 $Ca_V1.3$ hetero-clusters at intracellular membranes of the ER, at ER exit sites, and at the Golgi.
103 We also investigated the proximity between mRNA transcripts of BK and $Ca_V1.3$.

104

105 **Definitions used in this manuscript**

106 To guide the reader and prevent confusion on the terms used, we introduce the following
107 nomenclature, which is also illustrated in Figure 1. Molecular complex: an array of several
108 polypeptides with a defined function. In our case, a BK channel is a molecular complex of four
109 alpha subunits whose function is to permeate ions. Homo-cluster: we define a homo-cluster as
110 the accumulation of proteins. In our work, a homo-cluster refers to the accumulation of BK
111 channels or the accumulation of calcium channels.

112 Hetero-cluster: we define a hetero-cluster as the collection of different types of proteins
113 that facilitate functional coupling and compartmentalization of a signaling complex. In the present
114 work, hetero-cluster refers to a coordinated collection of BK and Ca_V channels. It is also used to
115 refer to the assembly of homo-clusters of BK with homo-clusters of Ca_V channels.

116

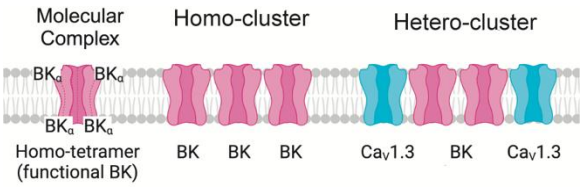

Figure 1. Representation of molecular complex, homo-cluster, and hetero-cluster.

117

118 **Materials and Methods**

119 **Cell culture:**

120 We used tsA-201 cells to co-express BK and $Ca_V1.3$ channels heterologously. Cells were
121 grown in DMEM (Gibco) supplemented with 10% fetal bovine serum and 0.2%
122 penicillin/streptomycin. We used rat insulinoma (INS-1) cells to study endogenous levels of
123 transcripts and proteins of channels. INS-1 cells were cultured in RPMI high glutamate medium
124 (Gibco) with 10% fetal bovine serum, 0.2% penicillin/streptomycin, 10 mM HEPES (Gibco), 1 mM
125 sodium pyruvate (Gibco), and 50 μM 2-mercaptoethanol. Both cell types were passaged twice a
126 week and incubated in 5% CO_2 at 37°C.

127

128 **Plasmids and transfection:**

129 Cells were transfected with 0.1– 0.4 µg DNA per plasmid and plated for 24 hours on poly-
130 D-Lysine coated coverslips. Lipofectamine 3000 (Invitrogen, RRID: L30000) was used for the
131 transfection. DNA clones of $Ca_V1.3$, BK channels, PH-PLCδ GFP, ER moxGFP, pmGFP-Sec16S
132 and Golgi-mGFP were obtained from Addgene (RRID:SCR_002037). The $Ca_V1.3$ α subunit
133 construct used in our study corresponds to the rat $Ca_V1.3e$ splice variant containing exons 8a, 11,
134 31b, and 42a, with a deletion of exon 32. The BK channel construct corresponds to the VYR splice
135 variant of the mouse BKα subunit (KCNMA1). Auxiliary subunits for $Ca_V1.3$ channels, $Ca_Vβ3$ and
136 $Ca_Vα2δ1$ (from Diane Lipscombe, Brown University, RI), were transfected as well. No BK channel
137 auxiliary subunits were transfected.
138
139 **Antibodies:**
140 $Ca_V1.3$ channels were immuno-detected with a rabbit primary antibody recognizing
141 residues 809 to 825 located at the intracellular II-III loop of the channel
142 (DNKVTIDDYQEEAEDKD), kindly provided by Drs. William Catterall and Ruth Westenbroek [32].
143 BK channels were detected using the anti-Slo1 mouse monoclonal antibody clone L6/60. The
144 goat polyclonal GFP antibody was against the recombinant full-length protein corresponding to
145 *Aequorea victoria* GFP. Anti-58K Golgi protein antibody was used to mark the Golgi. Specificity
146 of antibodies was tested in un-transfected tsA-201 cells (Figure 2- Supplementary 1). The
147 secondary antibodies tagged with Alexa dyes were Donkey anti-mouse Alexa-647, Donkey anti-
148 rabbit Alexa-555, Donkey anti-goat Alexa-488 (Molecular Probes).
149
150 **Immunostaining:**
151 Cells were fixed with freshly prepared 4% paraformaldehyde for 10 minutes. After
152 washing, aldehydes were reduced with 0.1% $NaBH_4$ for 5 minutes and then washed again.
153 Nonspecific binding was blocked with 3% bovine serum albumin (Thermo Scientific). Cells were
154 permeabilized with 0.25% v/v Triton X-100 in PBS for 1 hour. Primary antibodies were used at 10
155 µg/ml in blocking solution and incubated overnight at 4°C. After washing, secondary antibodies
156 at 2 µg/ml were incubated for 1 hour at 21˚C. Washing steps indicated in all methods include 3
157 cycles of rinsing and rocking for 5 minutes with PBS at 21˚C. Cells were imaged using an inverted
158 AiryScan microscope or an ONI Nanoimager with super-resolution capabilities, in total internal
159 reflection fluorescence (TIRF) mode, and with a Z-resolution of 50 nm.
160
161 **Proximity ligation assay (PLA):**

162 Cells were fixed with freshly prepared 4% paraformaldehyde for 10 minutes. After
163 washing, aldehydes were reduced with 50 mM glycine for 15 minutes. After another round of
164 washes, PLA was performed according to manufacturer instructions (Duolink® In Situ Red Starter
165 Kit). Cells were blocked and permeabilized with Duolink blocking solution. Primary antibodies
166 were used at 10 µg/ml in Duolink antibody diluent and incubated overnight at 4°C. The Duolink®
167 In Situ PLA® probe anti-rabbit PLUS and anti-mouse MINUS were used as secondary antibodies,
168 followed by ligation and amplification. For PLA combined with immunostaining, PLA was followed
169 by a secondary antibody incubation with Alexa Fluor-488 at 2 µg/ml for 1 hour at 21˚C. Since GFP
170 fluorescence fades significantly during the PLA protocol, resulting in reduced signal intensity and
171 poor image resolution, GFP was labeled using an antibody rather than relying on its intrinsic
172 fluorescence. Coverslips were mounted using ProLong™ Gold Antifade Mountant with DAPI.
173 Cells were imaged using an inverted Zeiss AiryScan microscope.
174
175 **Single-molecule fluorescence in situ hybridization (RNAscope™):**
176 Manual RNAscope assay was performed using RNAscope Multiplex Fluorescent V2
177 Assay according to the manufacturer's protocol. The RNAscope assay consists of target probes
178 and a signal amplification system composed of a preamplifier, amplifier, and label probe. A
179 schematic RNAscope assay procedure is shown in Figure 5- Supplementary 1. Briefly, cells were
180 fixed with 4% paraformaldehyde for 30 minutes, washed, dehydrated, and then rehydrated with
181 ethanol, and permeabilized with 0.1% Tween-20 in PBS. Next, cells were quenched with H_2O_2
182 and treated with Protease III. Probes were hybridized for 2 hours at 40°C followed by RNAscope
183 amplification and then fluorescence detection. Coverslips were mounted using ProLong™ Gold
184 Antifade Mountant with DAPI. We used the following RNAscope probes: RNAscope 3-plex
185 Positive Control Probes, RNAscope 3-plex negative control probes, RNAscope™ Probe- Rn-Ryr,
186 RNAscope™ Probe- Rn-Scn9a, RNAscope Probe- Rn-Kcnma1-C3, RNAscope Probe- Rn-
187 Cacna1d-C2, and RNAscope Probe- Rn-Gapdh. Cells were imaged on the inverted AiryScan
188 microscope. For PLA and RNAscope experiments, we used custom-made macros written in
189 ImageJ. Processing of PLA data included background subtraction. To assess colocalization,
190 fluorescent signals were converted into binary images, and channels were multiplied to identify
191 spatial overlap. Specificity of RNAscope probes was tested in un-transfected tsA-201 cells (Figure
192 5- Supplementary 2). For RNAscope combined with immunostaining, RNAscope was followed by
193 blocking in PBS supplemented with 0.01 % Tween-20 and 3% BSA for 1 h at 21˚C. Samples were
194 then probed for BK protein using primary antibody overnight at 4˚C followed by secondary
195 antibody incubation with Alexa Fluor-488 at 2 µg/ml for 1 hour at 21˚C. Coverslips were mounted

196 using ProLong™ Gold Antifade Mountant. Cells were imaged using an inverted Zeiss AiryScan
197 microscope.
198
199 **High resolution imaging:**
200 Cells were imaged using an inverted AiryScan microscope (Zeiss LSM 880) run by ZEN
201 black v2.3 software and equipped with a plan apochromat 63X oil immersion objective with 1.4
202 NA. Fluorescent dyes were excited with a 405 nm diode, 458–514 nm argon, 561 nm, or 633 nm
203 laser. Emission light was detected using an Airyscan 32 GaAsP detector and appropriate
204 emission filter sets. The point spread functions were calculated using ZEN black software and 0.1
205 µm fluorescent microspheres. The temperature inside the microscope housing was 22°C. Images
206 were analyzed using ImageJ (NIH).
207
208 **Super-resolution imaging:**
209 Direct stochastic optical reconstruction microscopy (dSTORM) images of BK and $Ca_V1.3$
210 overexpressed in tsA-201 cells were acquired using an ONI Nanoimager microscope equipped
211 with a 100X oil immersion objective (1.4 NA), an XYZ closed-loop piezo 736 stage, and triple
212 emission channels split at 488, 555, and 640 nm. Samples were imaged at 35°C. For single-
213 molecule localization microscopy, fixed and stained cells were imaged in GLOX imaging buffer
214 containing 10 mM β-mercaptoethylamine (MEA), 0.56 mg/ml glucose oxidase, 34 µg/ml catalase,
215 and 10% w/v glucose in Tris-HCl buffer. Single-molecule localizations were filtered using NImOS
216 software (v.1.18.3, ONI). Localization maps were exported as TIFF images with a pixel size of 5
217 nm. Maps were further processed in ImageJ (NIH) by thresholding and binarization to isolate
218 labeled structures. To assess colocalization between the signal from two proteins, binary images
219 were multiplied. Particles smaller than 400 nm^2 were excluded from the analysis to reflect the
220 spatial resolution limit of STORM imaging (20 nm) and the average size of BK channels. To
221 examine spatial localization preference, binary images of BK were progressively dilated to 20 nm,
222 40 nm, 60 nm, 80 nm, 100 nm, and 200 nm to expand their spatial representation. These modified
223 images were then multiplied with the $Ca_V1.3$ channel to quantify colocalization and determine BK
224 occupancy at increasing distances from $Ca_V1.3$. To ensure consistent comparisons across
225 distance thresholds, data were normalized using the 200 nm measurement as the highest
226 reference value, set to 1.
227
228 **Image scrambling:**

229 Images were binarized as TIFF images, and their respective cell perimeter coordinates
230 were exported as CSV files by ImageJ. Processed binary images were then analyzed by our
231 SpotScrambler (https://github.com/jehuang2/SpotScramble) Python program. SpotScrambler first
232 extracts the areas of fluorescent particles in the binary image. SpotScrambler then redraws the
233 fluorescent particles as circles at randomized coordinates within cell perimeter boundaries.
234 SpotScrambler accurately preserves particle number and particle sizes, averaging less than 1%
235 difference in total area of fluorescent particles between pre-SpotScrambler and post-
236 SpotScrambler images. To ensure reliable randomization for each experiment, results were
237 averaged between 3 trials of SpotScrambler.
238
239 **Data analysis**
240 Excel (Microsoft), and Prism (GraphPad) were used to analyze data. ImageJ was used to
241 process images. One-way ANOVA and non-parametric statistical test (Mann-Whitney Wilcoxon)
242 were used to test for statistical significance. p-values <0.05 were deemed statistically significant.
243 The number of cells used for each experiment is detailed in each figure legend.
244
245 **Results**
246 **BK and Ca_V1.3 hetero-clusters are found inside the cell.**
247 BK and Ca_V hetero-clusters have been observed at the plasma membrane [14-16].
248 However, a clear understanding of when or how BK and Ca_V hetero-clusters assemble is missing.
249 A simple mechanism proposes that these hetero-clusters organize only at the plasma membrane.
250 Here, we tested the alternative hypothesis of BK and Ca_V assembling inside the cell (Figure 2A).
251 To test this idea, we used proximity ligation assay (PLA) and antibodies against BK and Ca_V1.3
252 channels. When these antibodies are within 40 nm of each other, PLA ligation and amplification
253 can occur, resulting in the formation of fluorescent puncta (Figure 2B), here referred to as PLA
254 puncta. Hence, the PLA puncta in Figure 2C represent BK and Ca_V1.3 hetero-clusters. To confirm
255 specificity, a negative control was performed by probing only for BK using the primary antibody,
256 ensuring that detected signals were not due to non-specific binding or background fluorescence.
257 We first analyzed Z-projections, in which all the puncta in the cell volume are added, and found a
258 density of 5.8 ± 1.0 / 10 μm^2. In a different experiment, we analyzed the puncta density for each
259 focal plane of the cell (step size of 300 nm) and compared the puncta at the plasma membrane
260 to the rest of the cell. We visualized the plasma membrane with a biological sensor tagged with
261 GFP (PH-PLCδ-GFP) and then probed it with an antibody against GFP (Figure 2E). By analyzing

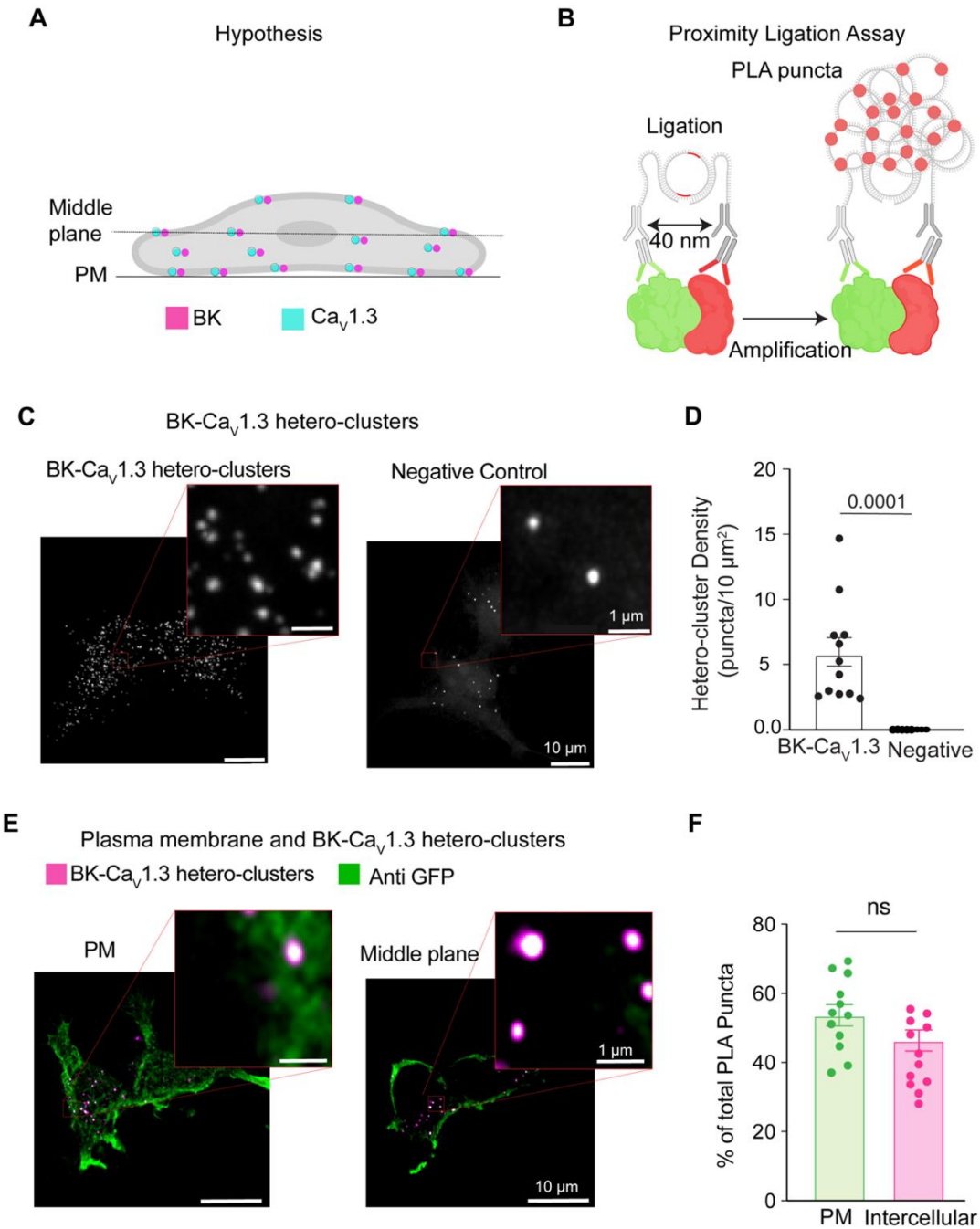

Figure 2. BK and Cav1.3 hetero-clusters are found inside the cell. A. Diagram of the hypothesis: hetero-clusters of BK (magenta) and Cav1.3 (cyan) are on intracellular membranes and on the plasma membrane. **B.** Illustration of the technique to detect BK and Cav1.3 hetero-clusters. Proximity ligation assay is used to detect the hetero-clusters. **C.** Confocal images of fluorescent puncta from PLA experiments in tsA-201 cells. Left: Cells were transfected and probed for BK and Cav1.3 channels. Right: negative control. Cells were transfected and probed only for BK channels. Enlargement of a selected region is shown in the inset. **D.** Scatter dot plot comparing puncta density of BK and Cav1.3 hetero-clusters to the negative control. Data points are from n = 12 cells for BK and Cav1.3 hetero-clusters and from n = 14 cells for negative control. *p*-values are shown at the top of the graphs. **E.** Confocal images of fluorescent PLA puncta at different focal planes co-labeled against GFP at the plasma membrane. Cells were transfected with BK, Cav1.3, and PH-PLCδ-GFP and probed for BK channels, Cav1.3 channels, and GFP. PLA puncta are shown in magenta, and the plasma membrane is shown in green. Enlargements of the representative regions of PM and intercellular hetero-clusters are shown in the insets. **F.** Scatter dot plot comparing BK and Cav1.3 hetero-cluster abundance at PM and inside the cell. Data points are from n = 12 cells. Scale bar is 10 µm and 1 µm in the insets. For statistical analysis, unpaired t-tests were applied in panel D and paired t-tests in panel F to evaluate significance.

263 the GFP signal, we created a mask that represented the plasma membrane. The mask served to
264 distinguish between the PLA puncta located inside the cell and those at the plasma membrane,
265 allowing us to calculate the number of PLA puncta at the plasma membrane. To our surprise, we
266 found a significant number of puncta localized inside the cell. 46 ± 3 % of the puncta were
267 localized intracellularly, whereas 54 ± 3 % were at the plasma membrane. This finding is
268 consistent with our supposition that BK and $Ca_V1.3$ channels colocalize in the cell.
269
270 **BK and $Ca_V1.3$ hetero-clusters localize at ER and ER exit sites.**
271 We next investigated the identity of the intracellular membranes where these PLA puncta
272 were found. A large component of intracellular membranes in the cell is the endoplasmic reticulum
273 (ER), where channels are inserted after translation. To determine whether BK and $Ca_V1.3$
274 associate in the ER (Figure 3A), we combined PLA with immunodetection. As before, PLA probed
275 for BK and $Ca_V1.3$ hetero-clusters, while a KDEL-moxGFP label identified the ER (Figure 3B). To
276 avoid disruption of organelle architecture, we used the monomeric mox version of KDEL-GFP,
277 which is optimized to reduce oligomerization in the ER environment [33]. Neither overexpression
278 of KDEL-moxGFP nor fixation altered the ER structure as the tubule width remained around 150
279 nm for either condition (Figure 3C), a value in agreement with the literature [34, 35]. To assess
280 the percentage of PLA puncta colocalizing with the ER, we employed two different cell lines, our
281 overexpression system (tsA-201 cells) and a rat insulinoma cell line (INS-1) that expresses BK
282 and $Ca_V1.3$ channels endogenously. In this and following experiments, we analyze one focal
283 plane, in the middle of the cell, to quantify PLA puncta colocalization with ER membrane. Figure
284 3D shows PLA puncta in the same space as the ER. Comparing the overexpression and
285 endogenous systems, 63 ± 3% versus 50 ± 6% of total PLA puncta were localized at the ER
286 (Figure 3E). To determine whether the observed colocalization between BK–$Ca_V1.3$ hetero-
287 clusters and the ER was not simply due to the extensive spatial coverage of ER labeling, we
288 labeled ER exit sites using Sec16-GFP and probed for hetero-clusters with PLA. This approach
289 enabled us to test whether the hetero-clusters were preferentially localized to ER exit sites, which
290 are specialized trafficking hubs that mediate cargo selection and direct proteins from the ER into
291 the secretory pathway. In contrast to
292 the more expansive ER network, which supports protein synthesis and folding, ER exit sites
293 ensure efficient and selective export of proteins to their target destinations. By quantifying the
294 proportion of BK and $Ca_V1.3$ hetero-clusters relative to total channel expression at ER exit sites,
295 we found 28 ± 3% colocalization in tsA-201 cells and 11 ± 2% in INS-1 cells (Figure 3F). While
296 the percentage of colocalization between hetero-clusters and the ER or ER exit sites alone cannot

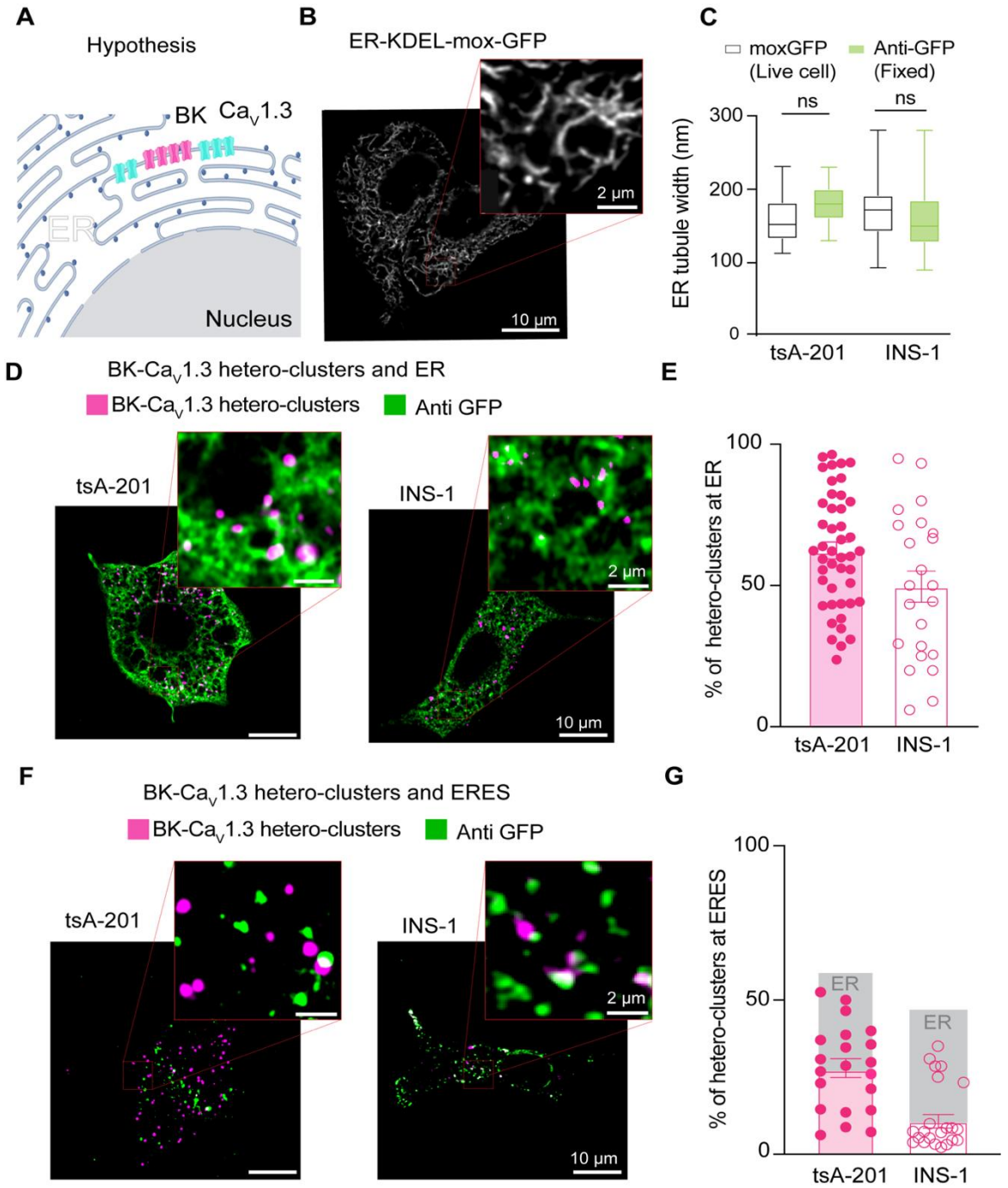

Figure 3. BK and Cav1.3 hetero-clusters localize at ER and ER exit sites (ERES). A. Diagram of the hypothesis: hetero-clusters of BK (magenta) and Cav1.3 (cyan) can be found at the ER membrane. **B.** Representative image of the ER labeled with exogenous GFP in INS-1 cells. Cells were transfected with KDEL-moxGFP. Magnification is shown in the inset. **C.** Comparison of the ER tubule distance in live and fixed tsA-201 and INS-1 cells. Data points are from n = 23 tsA-201 cells, n = 27 INS-1 cells **D.** Representative images of PLA puncta and ER. Left: tsA-201 cells were transfected with BK, Cav1.3 and KDEL-moxGFP. Right: INS-1 cells were transfected only with KDEL-moxGFP. Fixed cells were probed for BK-Cav1.3 hetero-clusters (PLA puncta) and GFP. PLA puncta is shown in magenta. ER is shown in green. **E.** Comparison of BK-Cav1.3 hetero-clusters found at the ER and relative to all PLA puncta in the cell. Values are given in percentages. **F.** Representative images of PLA puncta and ER exit sites. Left and right are the same as in D, but cells were transfected with Sec16-GFP instead of KDEL. **G.** Comparison of BK-Cav1.3 hetero-clusters found at ER exit sites relative to all PLA puncta in the cell. Values are given in percentages. Data points are from n = 45 tsA-201 cells for ER, n = 21 tsA-201 cells for ERES, n = 23 INS-1 cells for ER, and n = 23 INS-1 cells for ER exit sites. Scale bar is 10 µm and 2 µm in the magnifications.

297

298 be directly compared to infer trafficking dynamics, these findings reinforce the conclusion that
299 hetero-clusters reside within the ER and suggest that BK and $Ca_V1.3$ channels traffic together
300 through the ER and exit in coordination.
301
302 **BK and $Ca_V1.3$ hetero-clusters go through the Golgi.**
303 Channels are modified in the Golgi after synthesis (Figure 4A), so we asked whether PLA
304 puncta formed by BK and $Ca_V1.3$ hetero-clusters can be found in the Golgi. Using the same
305 strategy, we labeled Golgi with Gal-T-mEGFP (Figure 4B) and detected BK-$Ca_V1.3$ hetero-
306 clusters using PLA. To confirm that the overexpressed Gal-T-mEGFP labels the Golgi specifically
307 without altering its structure, we compared the region detected by the antibody against GFP to
308 the region detected by a primary antibody against the Golgi protein 58K (Figure 4C). 58K is a
309 specific peripheral protein that localizes to the cytosolic face of Golgi [36]. The overlay shows that
310 the GFP signal labels the same region as the antibody against 58K. When assessing the presence
311 of BK-$Ca_V1.3$ hetero-clusters in the Golgi, we found that 31 ± 5% of PLA puncta were localized at
312 the Golgi in the overexpression system and 25 ± 4% in the endogenous cell model (Figure 4E).
313 We performed controls to confirm that the formation of hetero-clusters between the two
314 channels was not coincidental but rather the result of structural coupling. We tested the formation
315 of PLA puncta between BK channels and the Golgi protein 58K. We also tested for $Ca_V1.3$ and
316 58K. We did not find PLA puncta when the proximity between the channels and 58K was probed
317 (Figure 4F), supporting the idea that PLA puncta between BK and $Ca_V1.3$ channels found at the
318 Golgi represent specific coupling. We selected the Golgi as a control because it represents the
319 final stage of protein trafficking, ensuring that hetero-cluster interactions observed at this point
320 reflect specificity maintained throughout earlier trafficking steps, including within the ER. As an
321 additional control, we tested the formation of PLA puncta between $Ca_V1.3$ channels and RyR_2, a
322 protein localized in the ER. The number of PLA puncta between $Ca_V1.3$ and RyR_2 was significantly
323 lower than the number observed between $Ca_V1.3$ and BK channels (Figure 4-Supplement 1),
324 further supporting the specificity of BK–$Ca_V1.3$ interactions.
325 It is important to clarify that the percentages provided in this work cannot be added up to
326 understand the distribution of hetero-clusters along the biosynthetic pathway of the channels. The
327 percentage in each membrane compartment was compared to the total percentage of hetero-
328 clusters observed in each cell for that particular experiment. Therefore, there is expected overlap
329 between our measurements due to (1) optical resolution and (2) the effect of not comparing all
330 the organelles in the same cell. Considering these limitations, we interpreted our results as
331 follows: about one half of hetero-clusters are found inside the cell. The other half corresponds to

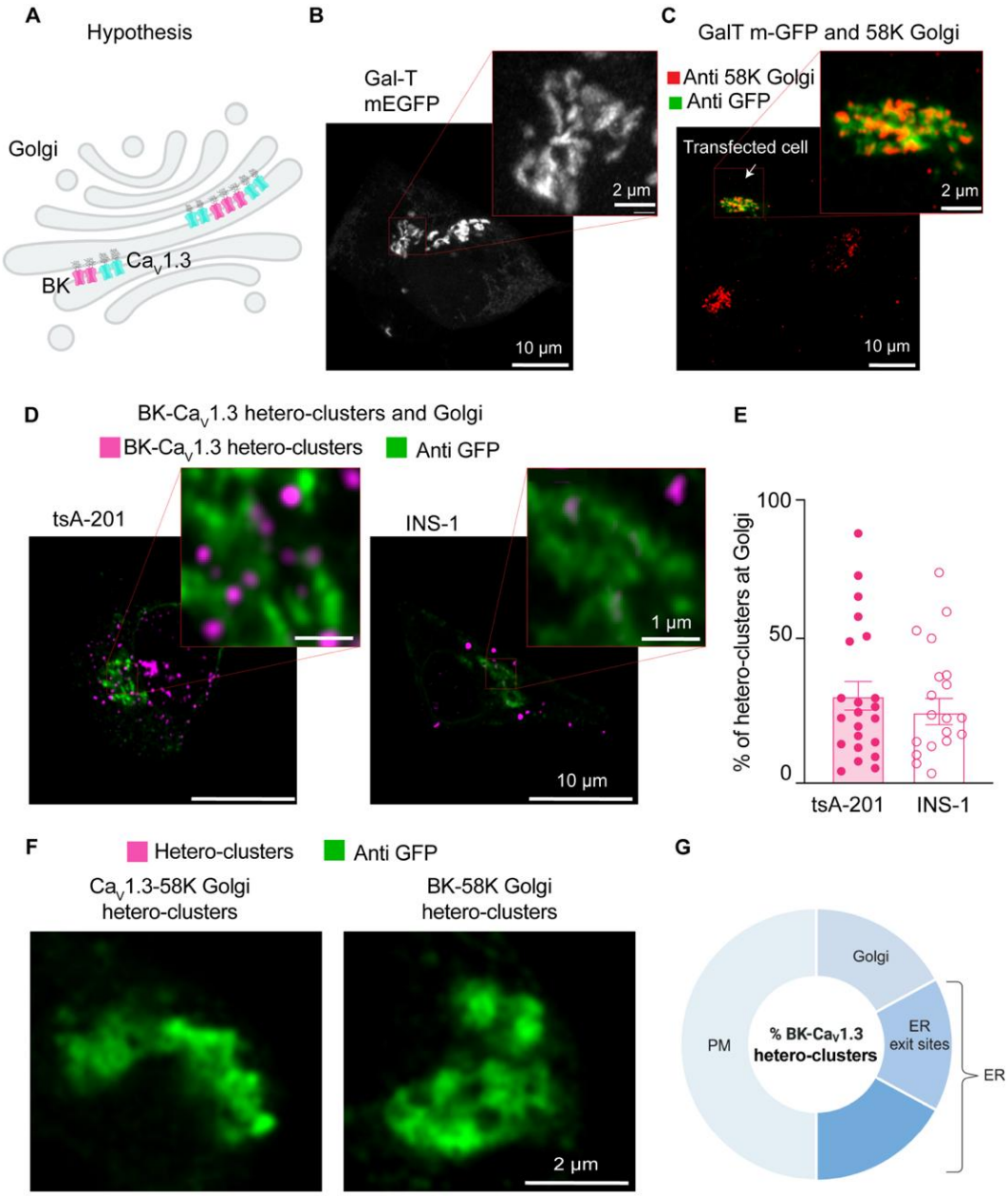

Figure 4. BK and Ca$_V$1.3 hetero-clusters go through the Golgi. A. Diagram of the hypothesis: PLA puncta detecting hetero-clusters between BK (magenta) and Ca$_V$1.3 (cyan) channels can be found at the Golgi membrane. **B.** Representative image of the Golgi structure with exogenous GFP in INS-1 cells. Cells were transfected with Gal-T-mEGFP. Enlargement is shown in the inset. **C.** Representative images of fixed cells co-stained with antibodies against Gal-T-mEGFP in green and 58K-Golgi in red **D.** Representative images of PLA puncta and Golgi. tsA-201 cells were transfected with BK, Ca$_V$1.3 and Gal-T-mEGFP (left), and INS-1 cells were transfected only with Gal-T-mEGFP (right). PLA puncta are shown in magenta. Golgi is shown in green. **E.** Scatter dot plot of percentages of BK-Ca$_V$1.3 hetero-clusters found at the Golgi relative to all PLA puncta in tsA-201 and INS1 cells. Data points are from n = 22 tsA-201 cells and n = 19 INS-1 cells. **F.** Representative image of PLA puncta and Golgi. tsA-201 cells were transfected with BK, Ca$_V$1.3, and Gal-T-mEGFP. Left: PLA was done against BK and 58K Golgi (magenta), and Golgi is shown in green. Right: PLA was done against Ca$_V$1.3 and 58K Golgi (magenta), and Golgi is shown in green. **G.** Diagram illustrating our interpretation of percentages of BK-Ca$_V$1.3 hetero-clusters found in the cell. This illustration is based on results shown in Figures 1-4. Percentages were modified to represent overlap of fluorescent signals and limited resolution. We also show that hetero-clusters found in the ER exit sites (ERES) are also accounted in the ER. Scale bars: 10 µm and 2 µm in panels B and C; 10 µm and 1 µm in panel D; 2 µm in panel F.

333 hetero-clusters at the plasma membrane. From the half inside the cell, roughly one third of hetero-
334 clusters is found in the Golgi, and another third is found in ER exit sites (Figure 4G). The remaining
335 hetero-clusters are found in other regions of the ER and in membranes that we did not probe,
336 such as vesicles. Finally, a key limitation of this approach is that we cannot quantify the proportion
337 of total BK or $Ca_V1.3$ channels engaged in hetero-clusters within each compartment. The PLA
338 method provides proximity-based detection, which reflects relative localization rather than
339 absolute channel abundance within individual organelles.
340
341 **BK mRNA and $Ca_V1.3$ mRNA colocalize.**
342 How is it that BK and $Ca_V1.3$ proteins come in close proximity in membranes of the ER,
343 ER exit sites and the Golgi? To explore the origins of the initial association, we hypothesized that
344 the two proteins are translated near each other, which could be detected as the colocalization of
345 their mRNAs (Figure 5A and B). The experiment was designed to detect single mRNA molecules
346 from INS-1 cells in culture. We performed multiplex in situ hybridization experiments using an
347 RNAscope fluorescence detection kit to be able to image three mRNAs simultaneously in the
348 same cell and acquired the images in a confocal microscope with high resolution. To rigorously
349 assess the specificity of this potential mRNA-level organization, we used
350 multiple internal controls. *GAPDH* mRNA, a highly expressed housekeeping gene with no known
351 spatial coordination with channel mRNAs, served as a baseline control for nonspecific
352 colocalization due to transcript abundance. To evaluate whether the spatial proximity between BK
353 mRNA (*KCNMA1*) and $Ca_V1.3$ mRNA (*CACNA1D*) was unique to functionally coupled channels,
354 we also tested for $Na_V1.7$ mRNA (*SCN9A)*, a transmembrane sodium channel expressed in INS-
355 1 cells but not functionally associated with BK. This allowed us to determine whether the observed
356 colocalization reflected a specific biological relationship rather than shared expression context.
357 Finally, to test whether this proximity might extend to other calcium sources relevant to BK
358 activation, we probed the mRNA of ryanodine receptor 2 (*RyR2*), another Ca^{2+} channel known to
359 interact structurally with BK channels [37]. Together, these controls were chosen to distinguish
360 specific mRNA colocalization patterns from random spatial proximity, shared subcellular
361 distribution, or gene expression level artifacts. Figure 5- Supplementary-2 shows images
362 completely void of fluorescent signal from INS-1 cells probed for bacterial mRNA (negative
363 control, Figure 5- Supplementary 2A) and shows images of INS-1 cells probed for mammalian
364 mRNAs expected to be in these cells (positive control, Figure 5- Supplementary 2B). The probes
365 against the mRNAs of interest and tested in this work were designed by Advanced Cell
366 Diagnostics. We confirmed the specificity of the probes by performing in situ hybridization against

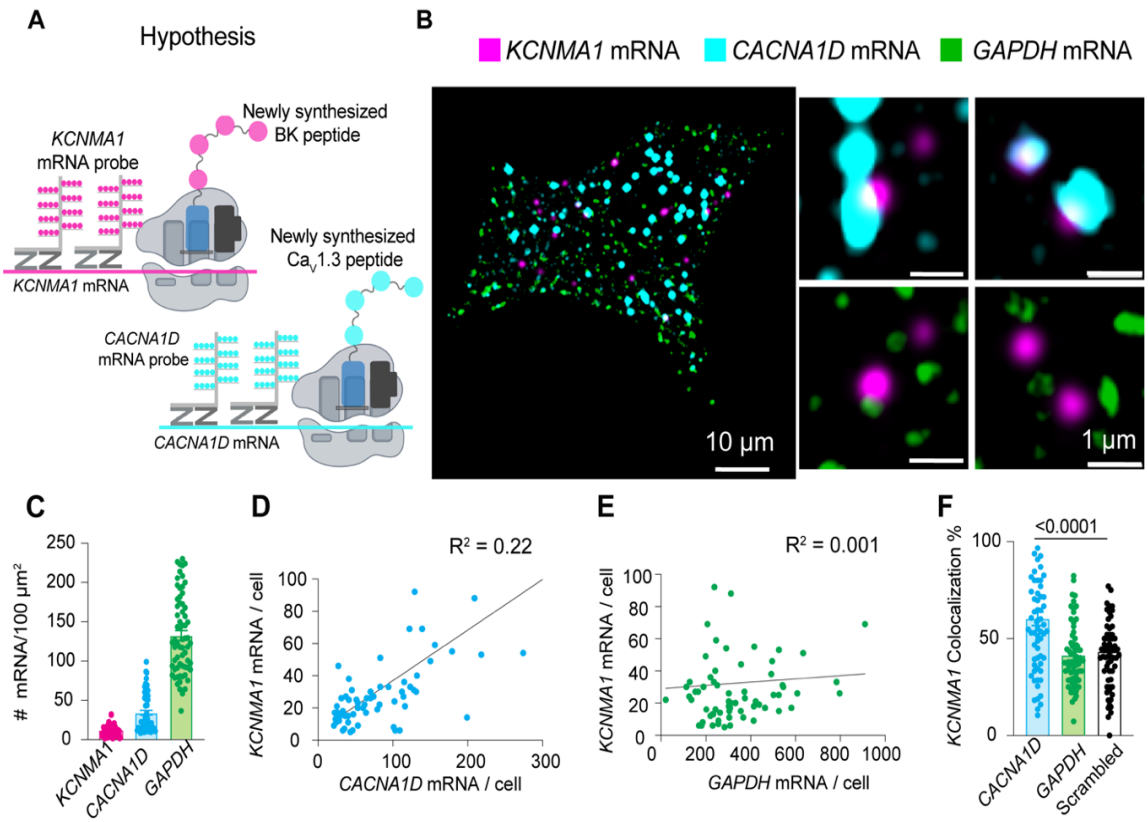

Figure 5. BK mRNA (*KCNMA1*) and $Ca_V1.3$ mRNA (*CACNA1D*) colocalize. A. Diagram of the hypothesis: *KCNMA1* and *CACNA1D* mRNAs are found in close proximity to be translated in the same neighborhood. **B.** Images of fluorescent puncta from RNA scope experiments showing *KCNMA1* mRNA in magenta, *CACNA1D* mRNA in cyan, and *GAPDH* mRNA in green. Right, magnification of three ROI. **C.** Comparison of mRNA density of *KCNMA1*, *CACNA1D*, and *GAPDH*. **D.** Correlation plot of mRNA abundance of *KCNMA1* and *CACNA1D* per cell. **E.** Correlation plot of mRNA abundance of *KCNMA1* and *GAPDH* per cell. **F.** Comparison of colocalization between *KCNMA1* mRNA and mRNA from *CACNA1D*, *GAPDH*, and scrambled images of *CACNA1D*. Data points are from n = 67 cells. Scale bar is 10 µm and 1 µm in the magnifications. Data were analyzed using ordinary one-way ANOVA with Dunnett's multiple comparisons test.

367 *KCNMA1*, *CACNA1D*, *RyR2*, and *SCN9A* in non-transfected cell lines (Figure 5- Supplementary
368 2C and D).

369 Probes against *GAPDH* mRNA were used as a control in the same cells that we probed
370 for *KCNMA1* and *CACNA1D* using the multiplex capability of this design. Transcripts were
371 detected at different expression levels. *GAPDH* and *CACNA1D* mRNAs were more abundant
372 (134 and 33 mRNA/100 μm^2, respectively) than *KCNMA1* mRNA (12 mRNA/100 μm^2, Figure 5C).
373 Interestingly, the abundance of *KCNMA1* transcripts correlated more with the abundance of
374 *CACNA1D* transcripts than with the abundance of *GAPDH*, though with a modest R^2 value (Figure

375 5D and E). Furthermore, *KCNMA1* and *CACNA1D* mRNA colocalized by 60 ± 4%, which was
376 20% more than with *GAPDH* mRNA (Figure 5F). As an additional control and to rule out the
377 potential influence of difference between *CACNA1D* and *KCNMA*1 abundance, we assessed
378 *CACNA1D* colocalization against randomized, computer-generated *KCNMA1* mRNA signals,
379 where localization was randomized while maintaining the same overall transcript count. The
380 significantly lower (20%) colocalization observed in scrambled conditions compared to genuine
381 BK-Cav1.3 mRNA interactions confirms that proximity is not an artifact of expression levels but
382 reflects a specific spatial association. These results suggest that some fraction of mRNAs for BK
383 and Ca_V1.3 channels are translated nearby, so the channel proteins potentially could be inserted

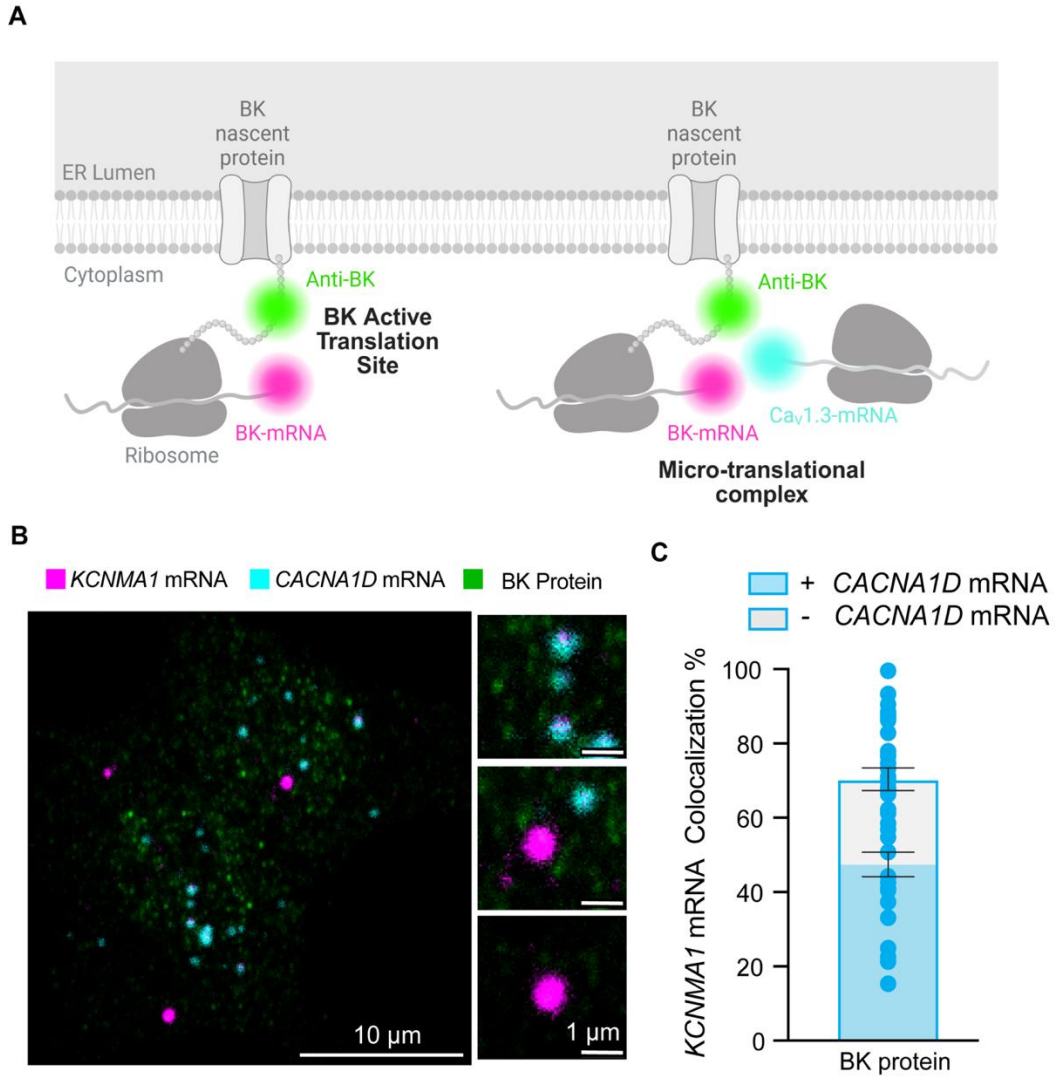

Figure 7. BK mRNA (*KCNMA1*) and Ca_V1.3 mRNA (*CACNA1D)* colocalize in micro-translational complexes. **A**. Diagram of the hypothesis: *KCNMA1* mRNAs are found in micro-translational complexes. **B.** Representative images of *KCNMA1* mRNA in magenta, *CACNA1D* mRNA in cyan, and BK protein in green. **C**. Comparison of the frequency of colocalization *KCNMA1* mRNA in active translation and in micro-translational complexes. Data points are from n = 57 cells. One way ANOVA was used as statistical analysis. Scale bar is 10 µm and 1 µm in the magnifications.

384 into the same regions of the ER. We suggest that the newly synthesized proteins remain together
385 during trafficking through the ER and the Golgi.

386 Next, we compared the proximity between *KCNMA1* and *SCN9A*. We detected *SCN9A* in
387 the same cells where *KCNMA1* was found (Figure 6A). The colocalization between *KCNMA1* and
388 *SCN9A* was only 18 ± 2% (Figure 6C), which was less than what was observed with *KCNMA1*
389 and *CACNA1D* (60%, Figure 5F). notably, We observed comparable levels of co-localization
390 between *KCNMA1* and *SCN9A* transcripts in both directions (data not shown), with no statistically
391 significant difference. These findings support the specificity of mRNA co-localization and that
392 *KCNMA1* tends to localize closer to *CACNA1D* than to *SCN9A* or *GAPDH*, supporting the
393 specificity of *KCNMA1* and *CACNA1D* mRNA association.

394 With the goal of understanding if this concept could apply to other channels, we used the
395 same approach to test a second protein known to provide calcium for BK channel opening. Similar
396 to the coupling between BK and $Ca_V1.3$ channels, RyR2 also can be structurally coupled to BK
397 channels [37]. Figure 6B shows high resolution images of single molecule in situ hybridization for
398 *RyR2* probed together with *KCNMA1* in INS-1 cells. In the same population of cells, *KCNMA1*
399 and *RyR2* colocalization was 27 ± 3%, which is 1.5 times that with *SCN9A* mRNA. We also
400 assessed *RyR2* colocalization with randomized, computer-generated *KCNMA1* mRNA signals.
401 We found that colocalization between randomized *KCNMA1* and genuine *RyR2* was 87% less

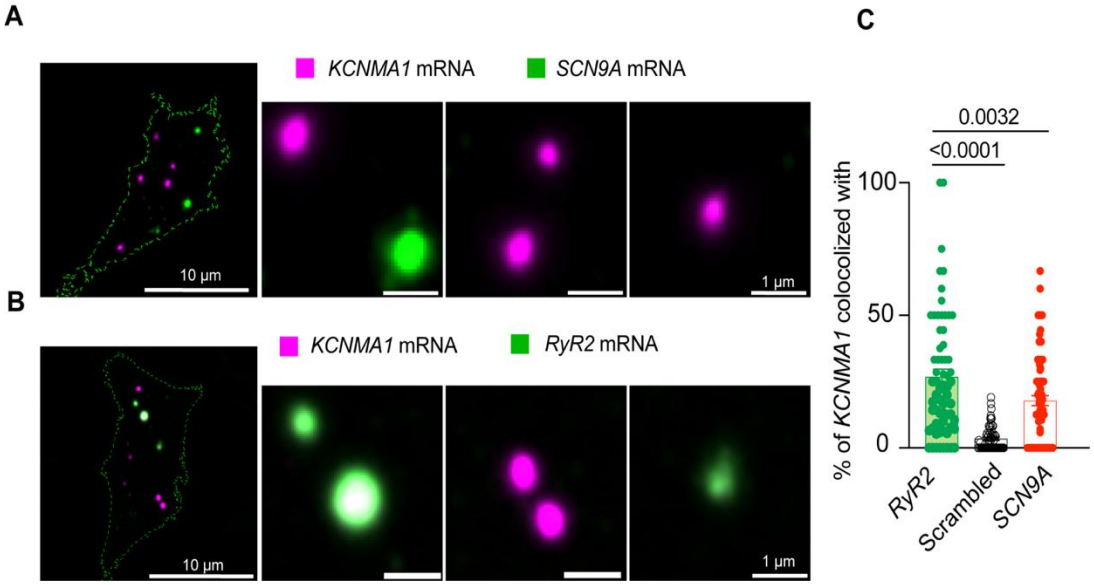

Figure 6. BK mRNA (*KCNMA1*) and RyR-2 mRNA (*RyR2*) colocalize. A. Representative confocal images of *KCNMA1* and $Na_V1.7$ (*SCN9A*) mRNA. **B.** Representative images of *KCNMA1* and *RyR2* mRNA. **C**. Comparison of the colocalization between *KCNMA1* mRNA and mRNA from *RyR2*, *SCN9A*, and scrambled images of *KCNMA1*. Data points are from n =67 cells. One way ANOVA. Scale bar is 10 µm and 1 µm in the magnifications. Data were analyzed using ordinary one-way ANOVA with Dunnett's multiple comparisons test.

402 colocalized compared to the analysis of genuine *KCNMA1* and genuine *RyR2* (Figure 6C),
403 suggesting that *KCNMA1* not only colocalizes with *CACNA1D* but also with mRNA of other known
404 calcium sources.

405 To further investigate whether *KCNMA1* and *CACNA1D* are localized in regions of active
406 translation (Figure 7A), we performed RNAscope targeting *KCNMA1* and *CACNA1D* alongside
407 immunostaining for BK protein. This strategy enabled us to visualize transcript-protein
408 colocalization in INS-1 cells with subcellular resolution.

409 By directly evaluating sites of active BK translation, we aimed to determine whether newly
410 synthesized BK protein colocalized with *CACNA1D* mRNA signals (Figure 7A). Confocal imaging
411 revealed distinct micro-translational complex where *KCNMA1* mRNA puncta overlapped with BK
412 protein signals and were located adjacent to *CACNA1D* mRNA (Figure 7B). Quantitative analysis
413 showed that 71 ± 3% of all *KCNMA1* colocalized with BK protein signal which means that they
414 are in active translation. Interestingly, 69 ± 3% of the *KCNMA1* in active translation colocalized
415 with *CACNA1D* (Figure 7C), supporting the existence of functional micro-translational complexes
416 between BK and $Ca_V1.3$ channels.

417

418 **BK and $Ca_V1.3$ channels form hetero-clusters at the plasma membrane of**
419 **INS-1 cells.**

420 We previously showed the organization of BK and $Ca_V1.3$ channels in hetero-clusters in
421 tsA-201 cells and neurons, including hippocampal and sympathetic motor neurons [15]. Our
422 present study utilizes INS-1 cells. We detected single microscopy and determined their degree of
423 colocalization. Figure 8A shows a representative image of the localizations of antibodies against
424 BK and $Ca_V1.3$ channels. Maps were rendered at 5 nm, the pixel size for the images presented.
425 BK-positive pixels formed multi-pixel aggregates, which has been interpreted as homo-clusters of
426 molecules in INS-1 cells. It is important to note that this technique does not allow us to distinguish
427 between labeling of four BK α-subunits within a tetramer and labeling of multiple BK channels in
428 a cluster. Hence, particles smaller than ~1680 nm² may represent either a single tetramer or a
429 cluster. This limitation applies to Figures 8C and 9D and does not affect measurements of BK–
430 $Ca_V1.3$ proximity. $Ca_V1.3$ channels also formed homo-clusters. When looking at the formation of
431 BK and $Ca_V1.3$ hetero-clusters, no fixed geometry or stoichiometry was observed. On the
432 contrary, maps showed a distribution of distances between BK and $Ca_V1.3$ detected pixels. In
433 some cases, BK and $Ca_V1.3$ channels were perfectly overlapping, as if the detection of the
434 antibodies could not be separated by the 20 nm resolution. In other cases, BK and $Ca_V1.3$

435 channels were adjacent (less than 5 nm), and in other cases, BK homo-clusters were surrounded
436 by a variable number of $Ca_V1.3$ channels.
437 To provide a more quantitative description of the maps, we measured cluster density,
438 cluster size, and colocalization. We used the particle analysis tool of the software ImageJ for
439 these measurements. In this analysis, a particle for represents positive pixels irrespective of the
440 number of pixels composed. INS-1 cells showed 4 times as many $Ca_V1.3$ particles as BK particles
441 (Figure 8B). Figure 8C shows the frequency distribution of particle size, where the median area
442 is 1691 nm^2 for BK and 975 nm^2 for $Ca_V1.3$. The colocalization between BK and $Ca_V1.3$ clusters
443 (Figure 8D) was 7.5%, a value higher than that obtained from scrambled image controls. Notably,

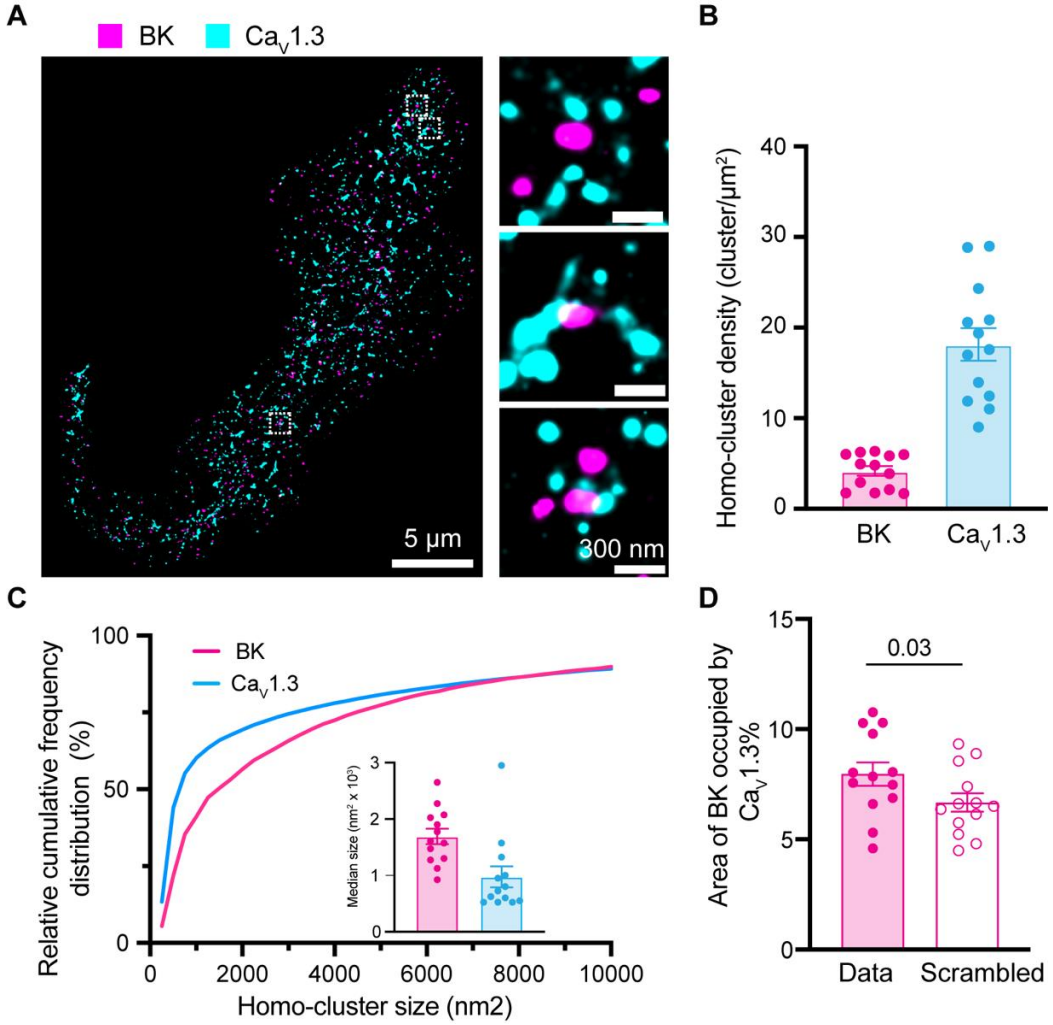

Figure 8. Formation of BK and $Ca_V1.3$ hetero-clusters in INS-1 cells. A. Representative localization map of antibodies against BK (magenta) and $Ca_V1.3$ (cyan) channels. Magnifications are shown in the insets on the right. **B.** Scatter dot plot of homo-cluster densities of BK and $Ca_V1.3$ channels in INS-1 cells. **C.** Cumulative frequency distributions of homo-cluster sizes of BK and $Ca_V1.3$ channels. Inset compares median size of BK and $Ca_V1.3$ homo-clusters. **D.** Comparison of colocalization between BK and $Ca_V1.3$ and between scrambled BK and $Ca_V1.3$. Data points are from n = 13 cells. Scale bar is 5 µm and 300 nm in the magnifications. Data was analyzed using paired t-tests to evaluate significance.

444 37 ± 3% BK channels are at 200 nm or less from one or more $Ca_V1.3$, while 15 ± 2% of $Ca_V1.3$
445 channels are at 200 nm or less from one or more BK (Figure 8-supplementary 1 Panel A).
446 Furthermore, the distribution of the nearest distance between BK and $Ca_V1.3$ in INS-1 cells
447 (Figure 8-supplementary 1 Panel B, magenta) shows a large proportion of BK channels (around
448 40%) at <50 nm from any $Ca_V1.3$ channels. Together, these results suggest that INS-1 cells also
449 exhibit nanodomains containing BK-$Ca_V1.3$ hetero-clusters at the plasma membrane.
450
451 **Hetero-clusters of BK and $Ca_V1.3$ channels are detected at the plasma membrane soon**
452 **after their expression.**
453 In light of our results, our current model is that BK and $Ca_V1.3$ hetero-clusters form prior
454 to their insertion into the plasma membrane. One prediction based on this model is that channels
455 inserted in the plasma membrane would appear as hetero-clusters already at early time points
456 after the start of their synthesis. To test this prediction, we transfected tsA-201 cells with BK and
457 $Ca_V1.3$ channels and performed a chase experiment to detect their presence at the plasma
458 membrane using super-resolution microscopy. We measured particle size, density, and
459 colocalization at 18, 24, and 48 hours after transfection. Notably, although the channels were
460 transfected simultaneously, BK particles were detected in the plasma membrane 18 hours after
461 transfection, whereas $Ca_V1.3$ particles were detected 24 hours after transfection (Figure 9A-C).
462 The distribution of BK and $Ca_V1.3$ particle size did not change with the time after transfection
463 (Figure 9D and E), in agreement with Sato et al., 2019 [30].
464 In support of our prediction, we found particles of $Ca_V1.3$ near BK particles as soon as the
465 expression of $Ca_V1.3$ channels was detected in the plasma membrane (24 hours after
466 transfection, enlarged Figure 9B). To test this hypothesis further, we compared plots of
467 localization preference at 24 and 48 hours. These plots were constructed by measuring the
468 percentage of $Ca_V1.3$ area occupying concentric regions of 20 nm width around BK particles.
469 Values were normalized to the percentage of colocalization found at 200 nm from BK. Figure 9F
470 shows that the localization preference plots are identical at 24 and 48 hours, consistent with the
471 hypothesis that both channels are inserted together into the plasma membrane already as hetero-
472 clusters.

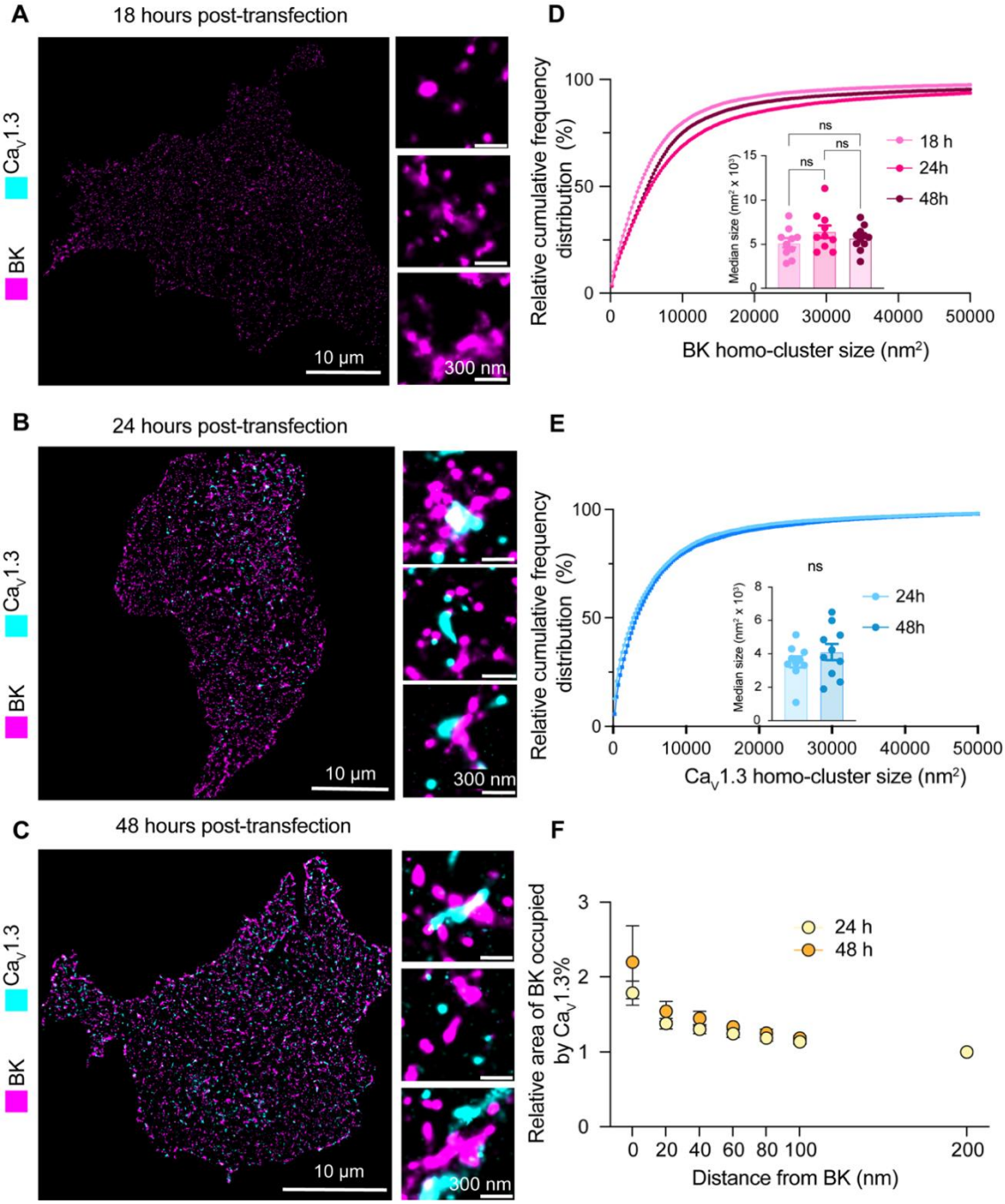

Figure 9. Hetero-clusters of BK and Ca$_V$1.3 channels are detected at the plasma membrane soon after their expression begins. A-C. Representative localization maps of antibodies against BK and Ca$_V$1.3 channels. (A) 18 hours, (B) 24 hours, or (C) 48 hours after DNA transfection into cells. Enlargements are shown in insets. **D.** Cumulative frequency distributions of BK homo-cluster size at 18, 24, and 48 hours. Inset compares median BK homo-cluster areas. **E.** Cumulative frequency distributions of Ca$_V$1.3 homo-clusters at 24 and 48 hours. Inset compares median Ca$_V$1.3 cluster areas. Ca$_V$1.3 clusters are not present at the 18-hour time point. **F.** Comparison of colocalization plots between BK and Ca$_V$1.3 channels at 24 and 48-hour time points. Data points are from n = 10 cells. Scale bar is 10 µm and 300 nm in enlargements. Statistical significance was assessed using ordinary one-way ANOVA followed by Dunnett's multiple comparisons test and unpaired t-test in panel D and E respectively.

473

Discussion

Intracellular Assembly of BK and $Ca_V1.3$ Channels

Previous work from our group has revealed the organization of hetero-clusters of large-conductance calcium-activated potassium (BK) channels and voltage-gated calcium channels, particularly $Ca_V1.3$, within nanodomains. This spatial organization is crucial for the functional coupling that enables BK channels to respond promptly to calcium influx, thereby modulating cellular excitability. While physical details of BK-$Ca_V1.3$ interactions are not fully elucidated, the evidence suggests that BK channels interact with both the Ca_V α1 subunit and its auxiliary subunits [38, 39].

Our findings highlight the intracellular assembly of BK-$Ca_V1.3$ hetero-clusters, though limitations in resolution and organelle-specific analysis prevent precise quantification of the proportion of intracellular complexes that ultimately persist on the cell surface. While our data confirms that hetero-clusters form before reaching the plasma membrane, it remains unclear whether all intracellular hetero-clusters transition intact to the membrane or undergo rearrangement or disassembly upon insertion. Future studies utilizing live cell tracking and high resolution imaging will be valuable in elucidating the fate and stability of these complexes after membrane insertion.

A stochastic model of ion channel homo-cluster formation in the plasma membrane proposes that random yet probabilistic interactions between ion channels contribute to their formation [30]. These clusters are stabilized and organized within specific membrane regions through biophysical mechanisms such as membrane curvature. Recent findings on spatial organization of G-protein coupled receptors provide additional support for this framework, demonstrating that the coupling of membrane proteins to the curvature of the plasma membrane acts as a driving force for their clustering into functional domains [40]. Yet, the mechanisms regulating the spatial organization of hetero-clusters are less known.

Colocalization and Trafficking Dynamics

The colocalization of BK and $Ca_V1.3$ channels in the ER and at ER exit sites before reaching the Golgi suggests a coordinated trafficking mechanism that facilitates the formation of multi-channel complexes crucial for calcium signaling and membrane excitability [41, 42]. Given the distinct roles of these compartments, colocalization at the ER and ER exit sites may reflect transient proximity rather than stable interactions. Their presence in the Golgi further suggests that post-translational modifications and additional assembly steps occur before plasma membrane transport, providing further insight into hetero-cluster maturation and sorting events.

508 By examining BK-Ca_V1.3 hetero-cluster distribution across these trafficking compartments, we
509 ensure that observed colocalization patterns are considered within a broader framework of
510 intracellular transport mechanisms [43]. Previous studies indicate that ER exit sites exhibit
511 variability in cargo retention and sorting efficiency [44], emphasizing the need for careful
512 evaluation of colocalization data. Accounting for these complexities allows for a robust
513 assessment of signaling complexes formation and trafficking pathways.
514
515 **BK Surface Expression and Independent Trafficking Pathways**
516 BK surface expression in the absence of Ca_V1.3 indicates that its trafficking does not
517 strictly rely on Ca_V1.3-mediated interactions. Since BK channels can be activated by multiple
518 calcium sources, their presence in intracellular compartments suggests that their surface
519 expression is governed by intrinsic trafficking mechanisms rather than direct calcium-dependent
520 regulation. While some BK and Ca_V1.3 hetero-clusters assemble into signaling complexes
521 intracellularly, other BK channels follow independent trafficking pathways, demonstrating that
522 complex formation is not obligatory for all BK channels. Differences in their transport kinetics
523 further reinforce the idea that their intracellular trafficking is regulated through distinct
524 mechanisms. Studies have shown that BK channels can traffic independently of Ca_V1.3, relying
525 on alternative calcium sources for activation [13, 45]. Additionally, Ca_V1.3 exhibits slower
526 synthesis and trafficking kinetics than BK, emphasizing that their intracellular transport may not
527 always be coordinated. These findings suggest that BK and Ca_V1.3 exhibit both independent and
528 coordinated trafficking behaviors, influencing their spatial organization and functional interactions.
529 Future experiments using inducible constructs to precisely control transcription timing will enable
530 more precise quantification of hetero-cluster formation in the ER compartment prior to plasma
531 membrane insertion and reduce the variability introduced by differences in expression timing after
532 plasmid transfection.
533
534 **mRNA Colocalization and Protein Trafficking**
535 The colocalization of mRNAs encoding BK and Ca_V1.3 channels suggests a coordinated
536 translation mechanism that facilitates their proximal synthesis and subsequent assembly into
537 functional complexes. As a mechanism, mRNA localization enhances protein enrichment at
538 functional sites, coordinating with translational control to position ion channels at specific
539 subcellular domains; ion channel positioning is especially critical for neurons and cardiomyocytes
540 [46, 47]. By synthesizing these channels in close proximity, channels can be efficiently assembled
541 into functional units, making this process crucial for precise targeting and trafficking of ion

542 channels to specific subcellular domains, thereby ensuring proper cellular function and efficient
543 signal transduction [48-50]. Disruption in mRNA localization or protein trafficking can lead to ion
544 channel mislocalization, resulting in altered cellular function and disease [51, 52]. In cardiac cells,
545 precise trafficking of ion channels to specific membrane subdomains is crucial for maintaining
546 normal electrical and mechanical functions, and its disruption contributes to heart disease and
547 arrhythmias [53-55] Similarly, in neurons, the localization and translation of mRNA at synaptic
548 sites are essential for synaptic plasticity, and disturbances can lead to neurological disorders [56,
549 57].
550

551 **Co-translational Regulation and Functional Coordination**

552 The potential co-translational association of transcripts encoding BK and $Ca_V1.3$ ion
553 channels, as well as other known calcium sources like RyR2, may serve as a mechanism to
554 ensure the precise stoichiometry and assembly of functional channel complexes. It is important
555 to note that while our data suggest mRNA coordination, additional experiments are required to
556 directly assess co-translation. In parallel, the spatial organization of BK channels with other
557 calcium sources such as RyR2—particularly in airway myocytes—has been shown to facilitate
558 efficient BK activation by localized Ca^{2+} sparks [38]. Co-translational association of transcripts
559 encoding $K_V1.3$ channels was the first example in which the interaction of nascent $K_V1.3$ N-termini
560 facilitates proper tertiary and quaternary structure required for oligomerization [58, 59]. Similarly,
561 co-translational heteromeric association of hERG1a and hERG1b subunits ensures that cardiac
562 IK_r currents exhibit the appropriate biophysical properties and magnitude necessary for normal
563 ventricular action potential shaping [51]. The precise mechanism by which BK transcripts are
564 associated with the transcripts of calcium sources like $Ca_V1.3$ and RyR2 channels remain to be
565 elucidated. While it is conceivable that complementary base pairing or tertiary structural
566 interactions play a role, RNA binding proteins (RBPs) are likely key mediators of these
567 associations.
568

569 **Conclusion and Future Directions**

570 This study provides novel insights into the organization of BK and $Ca_V1.3$ channels in
571 hetero-clusters, emphasizing their assembly within the ER, at ER exit sites, and within the Golgi.
572 Our findings suggest that BK and $Ca_V1.3$ channels begin assembling intracellularly before
573 reaching the plasma membrane, shaping their spatial organization, and potentially facilitating
574 functional coupling. While this suggests a coordinated process that may contribute to functional
575 coupling, further investigation is needed to determine the extent to which these hetero-clusters

576 persist upon membrane insertion. While our study advances the understanding of BK and $Ca_V1.3$
577 hetero-cluster assembly, several key questions remain unanswered. What molecular machinery
578 drives this colocalization at the mRNA and protein level? How do disruptions to complex assembly
579 contribute to channelopathies and related diseases? Additionally, a deeper investigation into the
580 role of RNA binding proteins in facilitating transcript association and localized translation is
581 warranted.
582
583 **Acknowledgments**

584 We thank Gail Robertson for her immense support and influence in designing and
585 conducting this project. We thank Alexey Merz for his support and feedback through this project.
586 We thank Bertil Hille for his contribution to editing the writing of this project. We thank Martina
587 Hunt, Maria Elena Danoviz, Paula Martinez-Feduchi, Wendy Piñon-Teal, and Raul Riquelme for
588 reading and providing feedback on the manuscript. We thank William Catterall and Ruth E.
589 Westenbroek for providing the antibody against $Ca_V1.3$. This study was supported by the National
590 Institutes of Health MIRA R35 GM142690 to O.V. C.M. was supported by HL162609 and the
591 Freeman Hrabowski HHMI Scholars program.
592

593 **Supplementary figures**

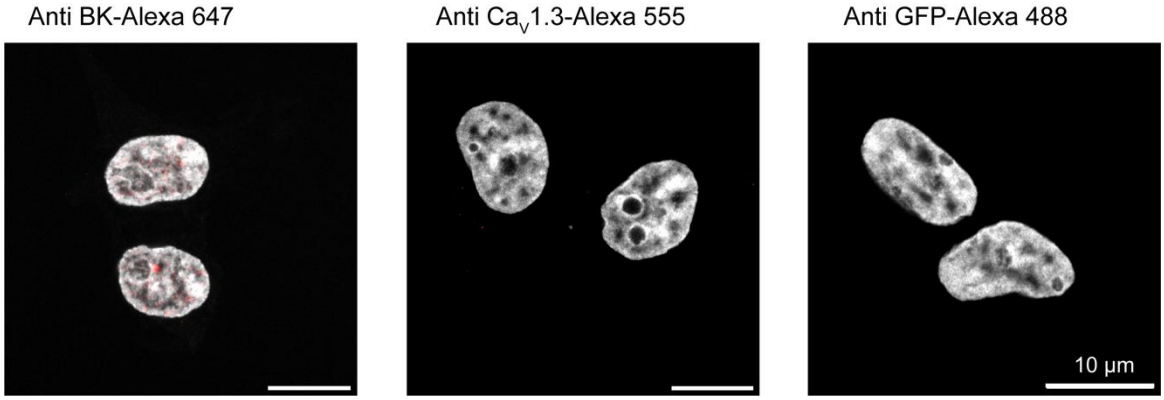

594

595 **Figure 2-Supplementary 1. Validation of antibodies against BK, Ca_V1.3 and GFP.** Representative confocal images
596 of tsA-201 cells immuno-tested for BK channels (left), Ca_V1.3 channels (middle), and GFP proteins (right). Cells were
597 not transfected. Nuclei were stained with DAPI and pseudo colored in gray. Scale bar is 10 µm for all images.

598

599

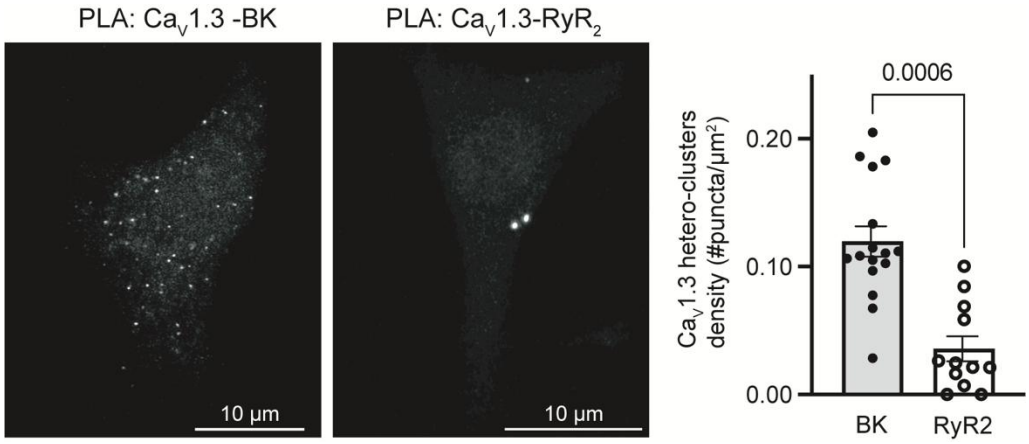

Figure 4-Supplementary 1. $Ca_V1.3$ channels do not exhibit proximity interactions with ryanodine receptor type 2 (RyR_2). A. Representative images of proximity ligation assay (PLA) experiments in INS-1 cells labeling against $Ca_V1.3$ and BK channels (left) or $Ca_V1.3$ and RyR_2 (right). Comparison of PLA puncta density for the two conditions. Statistical significance was assessed using an unpaired t-test.

608

609

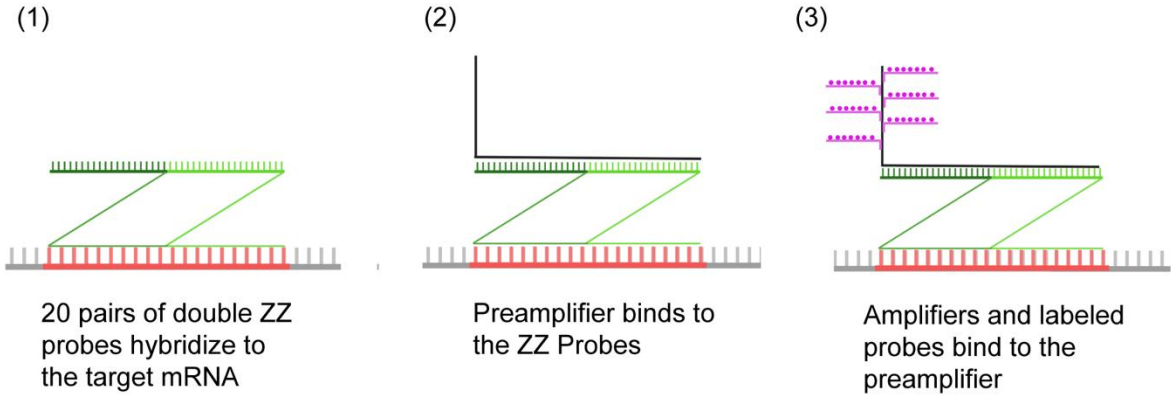

610

611 **Figure 5-Supplementary 1. Illustration of RNA scope methodology.** Steps to detect an mRNA sequence (red
612 zipper) consisting of (1) hybridization, (2) pre-amplification, (3) and labeling. Double ZZ probes are shown in green.
613 Dye labeling the mRNA is shown in magenta.

614

615

616
617

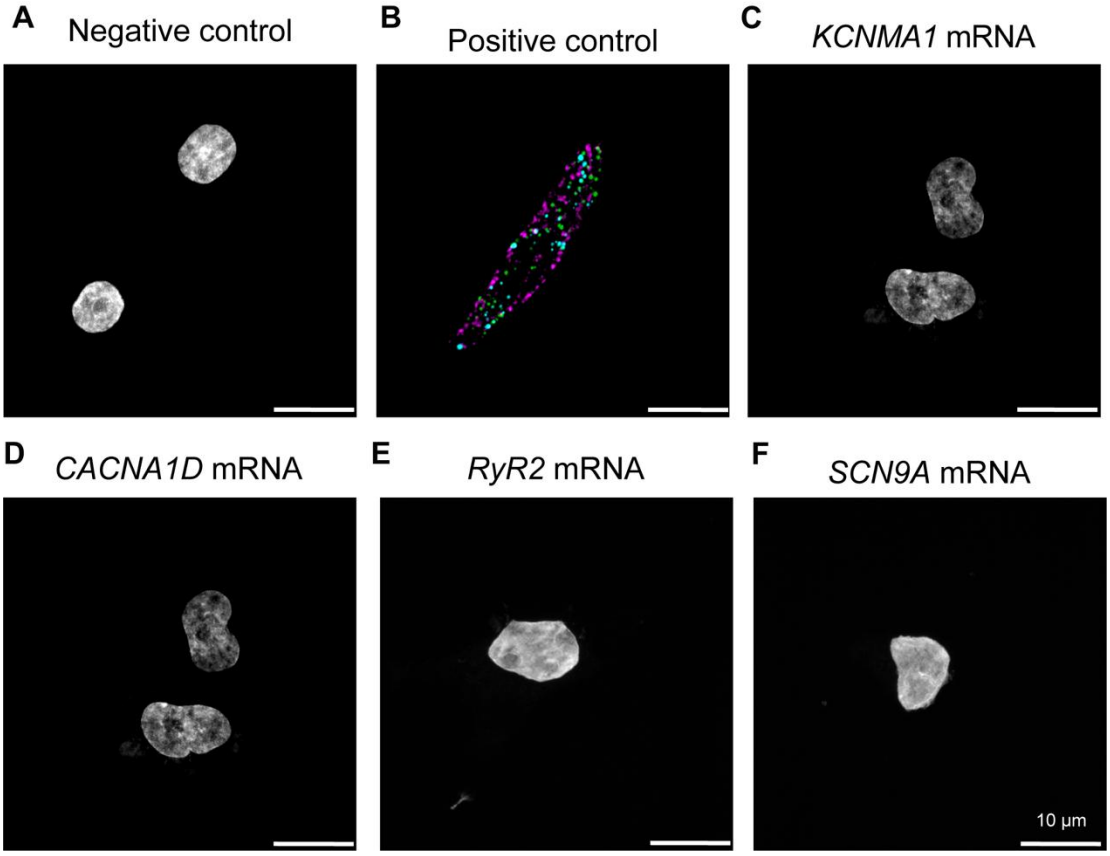

618
619 **Figure 5-Supplementary 2. RNA probe validation. A.** Representative images of INS-1 cells subjected to mRNA
620 probes against a bacterial gene (DapB from *Bacillus subtilis*). **B.** Representative images of INS-1 cells subjected to
621 mRNA probes against three constitutive mammalian genes (ubiquitin C, cyclophilin B, and a polymerase II subunit). **C**
622 **- F** show tsA-201 cells that were naive to exogenous DNA but treated with mRNA probes against the genes for (**C**)
623 BK channels, (**D**) $Ca_V1.3$ channels, (**E**) Ryanodine Receptors type 2 (RyR2), and (**F**) $Na_V1.7$ channels. Scale bar is
624 10 µm.
625
626

627
628

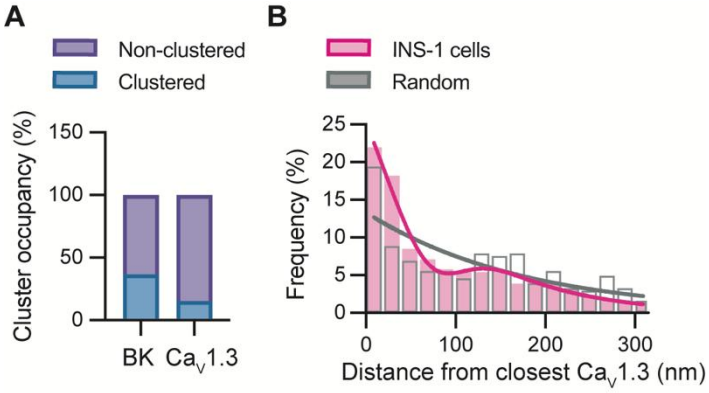

629
630 **Figure 8-Supplementary 1. Organization of BK-Ca$_V$1.3 hetero-clusters in INS-1 cells. A.** Proportion of channels in
631 clusters or outside clusters for BK and Ca$_V$1.3. Clustered channels were defined as being at a distance of 200 nm or
632 less from the other channel type. Channels found at 200 nm or more were considered non-clustered. Data from 7 cells.
633 **B.** Distribution of the nearest neighbor distance from BK channels to Ca$_V$1.3 channels in INS-1 cells (magenta, n =
634 1037 BK channels, from N = 5 cells). Distribution of the nearest neighbor distance from BK channels to randomized
635 channels (gray, n = 363 BK channels). The shift in the distribution from INS-1 cells to randomized images suggests a
636 preferential localization of endogenous BK-Ca$_V$1.3 hetero-clusters.
637
638

639 **Key Resources Table**

640

Reagent type	Designation	Source	Identifiers	Additional info.
Cell line	tsA-201	Sigma	RRID:CVCL_2737	
Cell line	INS-1	Sigma	RRID:CVCL_0352	
DNA clone	CaV1.3	Addgene	RRID:SCR_002037	Addgene ID: 49333
DNA clone	Slo1 (BK)	Addgene	RRID:SCR_002037	Addgene ID: 113566
DNA clone	KDEL-mox-GFP	Addgene	RRID:SCR_002037	Addgene ID: 68072
DNA clone	pmGFP-Sec16	Addgene	RRID:SCR_002037	Addgene ID: 15775
DNA clone	Golgi mGFP	Addgene	RRID:SCR_002037	Addgene ID: 182877
DNA clone	pPH-PLC-δ-GFP	Addgene	RRID:SCR_002037	Addgene ID: 51407
DNA clone	CaVβ3	Diane Lipscombe, Brown University		Auxiliary subunits for CaV1.3
DNA clone	CaVα2δ1	Diane Lipscombe, Brown University		Auxiliary subunits for CaV1.3
Genetic reagent	RNAscope 3-plex Positive Control Probes	Advanced Cell Diagnostics		Cat. No. 320871
Genetic reagent	RNAscope 3-plex Negative Control Probes	Advanced Cell Diagnostics		Cat. No. 320871
Genetic reagent	RNAscope™ Probe- Rn-Ryr	Advanced Cell Diagnostics		Cat. No. 2560931

Genetic reagent	RNAscope™ Probe- Rn-Scn9a	Advanced Cell Diagnostics		Cat. No. 317851
Genetic reagent	RNAscope Probe- Rn-Kcnma1-C3	Advanced Cell Diagnostics		Cat. No. 1108261-C3
Genetic reagent	RNAscope Probe- Rn-Cacna1d-C2	Advanced Cell Diagnostics		Cat. No. 409361-C2
Genetic reagent	RNAscope Probe- Rn-Gapdh	Advanced Cell Diagnostics		Cat. No. 409821
Antibody	Anti-CaV1.3	Drs. William Catterall and Ruth Westenbroek		rabbit primary antibody recognizing the residues 809 to 825 located at the intracellular II-III loop of the channel (DNKVTIDDYQEEAEDKD)
Antibody	Anti-Slo1	Millipore Sigma	RRID:AB_10805948	mouse monoclonal antibody clone L6/60, Cat. No. MABN70
Antibody	Anti GFP	abcam	RRID:AB_305643	corresponding to recombinant full length protein corresponding to *Aequorea victoria* GFP, Cat. No. ab6673
Antibody	Anti-58K Golgi	abcam	RRID:AB_2107005	Cat. No. ab27043
Antibody	Donkey anti-mouse-Alexa 647	Invitrogen	RRID:AB_2536183	Cat. No. A-31573
Antibody	Donkey anti-rabbit-Alexa 555	Invitrogen	RRID:AB_2534017	Cat. No. A10042
Antibody	Donkey anti-goat-Alexa 488	Invitrogen	RRID:AB_162542	Cat. No. A-31571
Antibody	Duolink® In Situ PLA®	Sigma	RRID:AB_2810940	

	probe anti-rabbit PLUS			
Antibody	Duolink® In Situ PLA® probe anti-mouse PLUS	Sigma	RRID:AB_2810939	
Commercial assay or kit	Duolink® In Situ Red Starter Kit	Sigma		Cat. No. DUO92008
Recombinant DNA reagent	Lipofectamine 3000	Invitrogen	RRID:L30000	
Reagent	ProLong™ Gold Antifade Mountant with DAPI	Invitrogen		Cat. No. P36931
Commercial assay or kit	RNAscope™ Multiplex Fluorescent V2 Assay	Advanced Cell Diagnostics		Cat. No. 323270
Software, algorithm	Prism	GraphPad	RRID:SCR_002798	
Software, algorithm	Excel	Microsoft		
Software, algorithm	ImageJ	NIH	RRID:SCR_003070	
Software, algorithm	NImOS software	ONI		v.1.18.3

641

642

643 **References:**

644

645 1. Contreras, G.F., et al., *A BK (Slo1) channel journey from molecule to physiology.*
646 Channels (Austin), 2013. **7**(6): p. 442-58.
647 2. Kaczorowski, G.J., et al., *High-conductance calcium-activated potassium channels;*
648 *structure, pharmacology, and function.* J Bioenerg Biomembr, 1996. **28**(3): p. 255-67.
649 3. Contet, C., et al., *BK Channels in the Central Nervous System.* Int Rev Neurobiol,
650 2016. **128**: p. 281-342.
651 4. Ancatén-González, C., et al., *Ca2+- and Voltage-Activated K+ (BK) Channels in the*
652 *Nervous System: One Gene, a Myriad of Physiological Functions.* Int J Mol Sci, 2023.
653 **24**(4).
654 5. Dopico, A.M., A.N. Bukiya, and J.H. Jaggar, *Calcium- and voltage-gated BK channels*
655 *in vascular smooth muscle.* Pflugers Arch, 2018. **470**(9): p. 1271-1289.
656 6. Hu, S.L., H.S. Kim, and A.Y. Jeng, *Dual action of endothelin-1 on the Ca2(+)-activated*
657 *K+ channel in smooth muscle cells of porcine coronary artery.* Eur J Pharmacol, 1991.
658 **194**(1): p. 31-6.
659 7. Semenov, I., et al., *BK channel beta1-subunit regulation of calcium handling and*
660 *constriction in tracheal smooth muscle.* Am J Physiol Lung Cell Mol Physiol, 2006.
661 **291**(4): p. L802-10.
662 8. Dupont, C., et al., *BK channels promote action potential repolarization in skeletal*
663 *muscle but contribute little to myotonia.* Pflugers Arch, 2024. **476**(11): p. 1693-1702.
664 9. Pallotta, B.S., K.L. Magleby, and J.N. Barrett, *Single channel recordings of Ca2+-*
665 *activated K+ currents in rat muscle cell culture.* Nature, 1981. **293**(5832): p. 471-4.
666 10. Meredith, A.L., *BK Channelopathies andand KCNMA1-Linked Disease Models.* Annu
667 Rev Physiol, 2024. **86**: p. 277-300.
668 11. Bailey, C.S., et al., *KCNMA1-linked channelopathy.* J Gen Physiol, 2019. **151**(10): p.
669 1173-1189.
670 12. Houamed, K.M., I.R. Sweet, and L.S. Satin, *BK channels mediate a novel ionic*
671 *mechanism that regulates glucose-dependent electrical activity and insulin secretion*
672 *in mouse pancreatic beta-cells.* J Physiol, 2010. **588**(Pt 18): p. 3511-23.
673 13. Shah, K.R., X. Guan, and J. Yan, *Structural and Functional Coupling of Calcium-*
674 *Activated BK Channels and Calcium-Permeable Channels Within Nanodomain*
675 *Signaling Complexes.* Front Physiol, 2021. **12**: p. 796540.

676 14. Berkefeld, H., et al., *BKCa-Cav channel complexes mediate rapid and localized Ca2+-*
677 *activated K+ signaling.* Science, 2006. **314**(5799): p. 615-20.
678 15. Vivas, O., et al., *Proximal clustering between BK and CaV1.3 channels promotes*
679 *functional coupling and BK channel activation at low voltage.* Elife, 2017. **6**.
680 16. Prakriya, M. and C.J. Lingle, *Activation of BK channels in rat chromaffin cells requires*
681 *summation of Ca(2+) influx from multiple Ca(2+) channels.* J Neurophysiol, 2000.
682 **84**(3): p. 1123-35.
683 17. Lipscombe, D., T.D. Helton, and W. Xu, *L-type calcium channels: the low down.* J
684 Neurophysiol, 2004. **92**(5): p. 2633-41.
685 18. Chen, G., et al., *BK channel modulation by positively charged peptides and auxiliary*
686 *γ subunits mediated by the Ca2+-bowl site.* Journal of General Physiology, 2023.
687 **155**(6).
688 19. Brenner, R., et al., Cloning and functional characterization of novel large conductance
689 calcium-activated potassium channel beta subunits, hKCNMB3 and hKCNMB4. J Biol
690 Chem, 2000. 275(9): p. 6453-61.
691 20. Dudem, S., et al., Oxidation modulates LINGO2-induced inactivation of large
692 conductance, Ca(2+)-activated potassium channels. J Biol Chem, 2023. 299(3): p.
693 102975.
694 21. Dudem, S., et al., LINGO1 is a regulatory subunit of large conductance,
695 Ca²⁺-activated potassium channels. Proceedings of the National
696 Academy of Sciences, 2020. 117(4): p. 2194-2200.
697 22. Knaus, H.G., et al., Primary sequence and immunological characterization of beta-
698 subunit of high conductance Ca(2+)-activated K+ channel from smooth muscle. J Biol
699 Chem, 1994. 269(25): p. 17274-8.
700 23. Yan, J. and R.W. Aldrich, LRRC26 auxiliary protein allows BK channel activation at
701 resting voltage without calcium. Nature, 2010. 466(7305): p. 513-6.
702 24. Yan, J. and R.W. Aldrich, BK potassium channel modulation by leucine-rich repeat-
703 containing proteins. Proceedings of the National Academy of Sciences, 2012. 109(20):
704 p. 7917-7922.
705 25. Liu, F., et al., *Cotranslational association of mRNA encoding subunits of heteromeric*
706 *ion channels.* Proc Natl Acad Sci U S A, 2016. **113**(17): p. 4859-64.
707 26. Eichel, C.A., et al., *A microtranslatome coordinately regulates sodium and potassium*
708 *currents in the human heart.* eLife, 2019. **8**: p. e52654.

709 27. Yang, S., et al., *Membrane curvature governs the distribution of Piezo1 in live cells.*
710 Nature Communications, 2022. **13**(1): p. 7467.
711 28. Chen, Z., et al., *EMC chaperone–CaV structure reveals an ion channel assembly*
712 *intermediate.* Nature, 2023. **619**(7969): p. 410-419.
713 29. Cheng, E.P., et al., *Restoration of Normal L-Type Ca2+ Channel Function During*
714 *Timothy Syndrome by Ablation of an Anchoring Protein.* Circulation Research, 2011.
715 **109**(3): p. 255-261.
716 30. Sato, D., et al., *A stochastic model of ion channel cluster formation in the plasma*
717 *membrane.* J Gen Physiol, 2019. **151**(9): p. 1116-1134.
718 31. Lu, J., et al., *T1-T1 interactions occur in ER membranes while nascent Kv peptides*
719 *are still attached to ribosomes.* Biochemistry, 2001. **40**(37): p. 10934-46.
720 32. Hell, J.W., et al., *Identification and differential subcellular localization of the neuronal*
721 *class C and class D L-type calcium channel alpha 1 subunits.* J Cell Biol, 1993. **123**(4):
722 p. 949-62.
723 33. Costantini, L.M., et al., *A palette of fluorescent proteins optimized for diverse cellular*
724 *environments.* Nat Commun, 2015. **6**: p. 7670.
725 34. Georgiades, P., et al., *The flexibility and dynamics of the tubules in the endoplasmic*
726 *reticulum.* Sci Rep, 2017. **7**(1): p. 16474.
727 35. Nixon-Abell, J., et al., *Increased spatiotemporal resolution reveals highly dynamic*
728 *dense tubular matrices in the peripheral ER.* Science, 2016. **354**(6311).
729 36. Bashour, A.M. and G.S. Bloom, *58K, a microtubule-binding Golgi protein, is a*
730 *formiminotransferase cyclodeaminase.* J Biol Chem, 1998. **273**(31): p. 19612-7.
731 37. Lifshitz, L.M., et al., *Spatial organization of RYRs and BK channels underlying the*
732 *activation of STOCs by Ca(2+) sparks in airway myocytes.* J Gen Physiol, 2011.
733 **138**(2): p. 195-209.
734 38. Rehak, R., et al., *Low voltage activation of KCa1.1 current by Cav3-KCa1.1*
735 *complexes.* PLoS One, 2013. **8**(4): p. e61844.
736 39. Zhang, F.X., et al., *BK Potassium Channels Suppress Cavα2δ Subunit Function to*
737 *Reduce Inflammatory and Neuropathic Pain.* Cell Rep, 2018. **22**(8): p. 1956-1964.
738 40. Kockelkoren, G., et al., *Molecular mechanism of GPCR spatial organization at the*
739 *plasma membrane.* Nat Chem Biol, 2024. **20**(2): p. 142-150.
740 41. Berkefeld, H., B. Fakler, and U. Schulte, Ca2+-activated K+ channels: from protein
741 complexes to function. Physiol Rev, 2010. 90(4): p. 1437-59.

742 42. Loane, D.J., P.A. Lima, and N.V. Marrion, Co-assembly of N-type Ca2+ and BK
743 channels underlies functional coupling in rat brain. J Cell Sci, 2007. 120(Pt 6): p. 985-
744 95.
745 43. Boncompain, G. and F. Perez, *The many routes of Golgi-dependent trafficking.*
746 Histochemistry and Cell Biology, 2013. **140**(3): p. 251-260.
747 44. Kurokawa, K. and A. Nakano, *The ER exit sites are specialized ER zones for the*
748 *transport of cargo proteins from the ER to the Golgi apparatus.* The Journal of
749 Biochemistry, 2019. **165**(2): p. 109-114.
750 45. Chen, A.L., et al., Calcium-Activated Big-Conductance (BK) Potassium Channels
751 Traffic through Nuclear Envelopes into Kinocilia in Ray Electrosensory Cells. Cells,
752 2023. 12(17): p. 2125.
753 46. Vacher, H., D.P. Mohapatra, and J.S. Trimmer, *Localization and targeting of voltage-*
754 *dependent ion channels in mammalian central neurons.* Physiol Rev, 2008. **88**(4): p.
755 1407-47.
756 47. Medioni, C., K. Mowry, and F. Besse, *Principles and roles of mRNA localization in*
757 *animal development.* Development, 2012. **139**(18): p. 3263-76.
758 48. Blandin, C.E., et al., *Remodeling of Ion Channel Trafficking and Cardiac Arrhythmias.*
759 Cells, 2021. **10**(9).
760 49. Dai, G., *Signaling by Ion Channels: Pathways, Dynamics and Channelopathies.* Mo
761 Med, 2023. **120**(5): p. 367-373.
762 50. Jameson, M.B., et al., *Pairwise biosynthesis of ion channels stabilizes excitability and*
763 *mitigates arrhythmias.* Proc Natl Acad Sci U S A, 2023. **120**(42): p. e2305295120.
764 51. Wang, E.T., et al., *Dysregulation of mRNA Localization and Translation in Genetic*
765 *Disease.* The Journal of Neuroscience, 2016. **36**(45): p. 11418.
766 52. Wang, J., et al., *RNA trafficking and subcellular localization—a review of mechanisms,*
767 *experimental and predictive methodologies.* Briefings in Bioinformatics, 2023. **24**(5):
768 p. bbad249.
769 53. Anderson, C.L., et al., *Most LQT2 mutations reduce Kv11.1 (hERG) current by a class*
770 *2 (trafficking-deficient) mechanism.* Circulation, 2006. **113**(3): p. 365-73.
771 54. Smyth, J.W. and R.M. Shaw, *Forward trafficking of ion channels: what the clinician*
772 *needs to know.* Heart Rhythm, 2010. **7**(8): p. 1135-40.
773 55. Basheer, W.A. and R.M. Shaw, *Connexin 43 and CaV1.2 Ion Channel Trafficking in*
774 *Healthy and Diseased Myocardium.* Circ Arrhythm Electrophysiol, 2016. **9**(6): p.
775 e001357.

776 56. Eliscovich, C., S.M. Shenoy, and R.H. Singer, *Imaging mRNA and protein interactions*
777 *within neurons.* Proc Natl Acad Sci U S A, 2017. **114**(10): p. E1875-E1884.
778 57. Yoon, Y.J., et al., *Glutamate-induced RNA localization and translation in neurons.* Proc
779 Natl Acad Sci U S A, 2016. **113**(44): p. E6877-E6886.
780 58. Robinson, J.M. and C. Deutsch, *Coupled tertiary folding and oligomerization of the T1*
781 *domain of Kv channels.* Neuron, 2005. **45**(2): p. 223-32.
782 59. Tu, L. and C. Deutsch, *Evidence for dimerization of dimers in K+ channel assembly.*
783 Biophys J, 1999. **76**(4): p. 2004-17.